

The L1615/L1616 PMS population: June 28, 2021

## The star formation in the L1615/L1616 Cometary Cloud

Davide Gandolfi<sup>1,2,3</sup>, Juan M. Alcalá<sup>2</sup>, Silvio Leccia<sup>2</sup>, Antonio Frasca<sup>1</sup>, Loredana Spezzi<sup>1,2</sup>,  
Elvira Covino<sup>2</sup>, Leonardo Testi<sup>4</sup>, Ettore Marilli<sup>1</sup>, Jouni Kainulainen<sup>5</sup>

### ABSTRACT

The present work aims at performing a comprehensive census and characterisation of the pre-main sequence (PMS) population in the cometary cloud L1615/L1616, in order to assess the significance of the triggered star formation scenario and investigate the impact of massive stars on its star formation history and mass spectrum. Our study is based on  $UBVR_CI_C$  and  $JHKs$  photometry, as well as optical multi-object spectroscopy. We performed a physical parametrisation of the young stellar population in L1615/L1616. We identified 25 new T Tauri stars mainly projected on the dense head of the cometary cloud, almost doubling the current number of known members. We studied the spatial distribution of the cloud members as a function of the age and  $H\alpha$  emission. The star formation efficiency in the cloud is  $\sim 7-8\%$ , as expected for molecular clouds in the vicinity of OB associations. The slope of the initial mass function (IMF), in the mass range  $0.1 \leq M \leq 5.5 M_\odot$ , is consistent with that of other T and OB associations, providing further support of an universal IMF down to the hydrogen burning limit, regardless of environmental conditions. The cometary appearance, as well as the high star formation efficiency, can be explained in terms of triggered star formation induced by the strong UV radiation from OB stars or supernovae shockwaves. The age spread as well as both the spatial and age distribution of the PMS objects provide strong evidence of sequential, multiple events and possibly still ongoing star formation activity in the cloud.

---

<sup>1</sup>INAF, Osservatorio Astrofisico di Catania, Via S. Sofia 78, 95123 Catania, Italy; dgandolfi@oact.inaf.it

<sup>2</sup>INAF, Osservatorio Astronomico di Capodimonte, Salita Moiariello 16, 80131 Napoli, Italy; jmae@na.astro.it

<sup>3</sup>Thüringer Landessternwarte Tautenburg, Sternwarte 5, 07778 Tautenburg, Germany; davide@tls-tautenburg.de

<sup>4</sup>INAF, Osservatorio Astronomico di Arcetri, L.go E. Fermi 5, 50125 Firenze, Italy; lt@arcetri.astro.it

<sup>5</sup>Observatory, PO Box 14, FIN-00014 University of Helsinki, Finland; jouni.kainulainen@helsinki.fi

*Subject headings:* cometary cloud: individual (L1615/L1616) — dust, extinction — stars: circumstellar matter — stars: formation — stars: fundamental parameters — stars: pre-main sequence

## 1. Introduction

The Lynds clouds L1615 and L1616 (Lynds 1962) are both located at an angular distance of about  $6^\circ$  West of the Orion OB1 associations. These clouds actually form a cometary-shaped single cloud with a “head-tail” distribution subtending about  $40'$  (5.2 pc assuming a distance of 450 pc; Alcalá et al. 2004) roughly in the East-West direction. The dense head of the cloud complex (i.e. L1616 only), pointing toward East and facing the bright Orion-belt stars, harbours the IRAS Small Scale Structure X0504-034 (Helou & Walker 1988; Ramesh 1995) and a bright reflection nebula, NGC 1788 (= DG 51, Ced 40, vdB 33, RNO 35, LBN 916; Lynds 1965), which is illuminated by a small cluster of stars (Stanke et al. 2002). The two intermediate-mass stars HD 293815 and Kiso A-0974 15 are the brightest visible members of this cluster.

L1615/L1616, like many other cometary clouds off the main Orion star forming regions, clearly shows evidence of ongoing star formation activity which might have been triggered by the strong impact of the UV radiation from the massive, luminous stars in the Orion complex (Maddalena et al. 1986; Stanke et al. 2002; Alcalá et al. 2004; Kun et al. 2004; Lee et al. 2005, 2007). The illumination of dense clumps in molecular clouds by OB stars could be responsible for their collapse and subsequent star formation. The UV radiation from the OB stars may sweep the molecular material of the cloud into a cometary shape with a dense core located at the head of the cometary cloud.

The radiation and wind of OB stars may also have an important impact on the mass accretion during the star formation process. While in a T association a protostar may accumulate a significant fraction of mass, the mass accretion of a low-mass protostar in a region exposed to the wind of OB stars can be terminated earlier because of the photo-evaporation of the circumstellar matter (Kroupa 2001, 2002). Therefore, many low-mass protostars may not complete their accretion and hence can result as brown dwarfs (BDs). This mechanism might affect the low-mass end of the initial mass function (IMF). Recent studies have provided some information about the shape of the IMF in the very low-mass and sub-stellar regimes. While the IMF in the Orion Nebula Cluster appears to rise below  $0.1 M_\odot$  (Hillenbrand & Carpenter 2000), in T association like Taurus-Auriga and Cha II there is some indication of a deficit of sub-stellar objects (Luhman et al. 2000; Briceño et al. 2002; Spezzi et al. 2008). Other studies of the young cluster IC 348, which is devoid of

very massive stars, have also revealed a deficit of BDs relative to the Orion Nebula Cluster (Preibisch et al. 2003; Muench et al. 2003; Lada et al. 2006).

Because of its vicinity to the Orion OB associations the L1615/L1616 cometary cloud constitutes an ideal laboratory to investigate the triggered star formation scenario. The most recent census of the pre-main sequence (PMS) stars in L1616 was provided by Alcalá et al. (2004), who presented a multi-wavelength study of the region, from X-ray to near-infrared wavelengths. They found 22 new low-mass PMS stars distributed mainly to the East of L1616, in about 1 square degree field. By adding the 22 new PMS stars to the previously confirmed members of the cloud (Cohen & Kuhi 1979; Sterzik et al. 1995; Nakano et al. 1995; Stanke et al. 2002) and counting the millimeter radio-source, i.e. the Class-0 protostar MMS1A found by Stanke et al. (2002), Alcalá et al. (2004) ended up with a sample of 33 young stellar objects associated with L1616. However, the latter work could not investigate important aspects of the star formation in this cloud, like the IMF and the impact of environmental conditions on the mass spectrum, because their sample was rather incomplete.

Therefore, the aim of the present study is to perform a comprehensive census and characterisation of the PMS population in L1615/L1616, in order to investigate the star formation history, the relevance of the triggered scenario, and to study the IMF. To this aim, we report both optical and near-infrared observations, as well as multi-object optical spectroscopy in L1615/L1616. An important goal of our study is to compare the mass function in L1615/L1616 with that of other T and OB associations.

The outline of the paper is as follows: we describe our observations and data reduction in Section 2 and 3; the results are reported in Section 4, while the data analysis and the physical proprieties of the new PMS stars are presented in Section 5. Our discussion and conclusions are developed in Section 6. Some details on the spectral-type classification as well as reddening, radius, and luminosity determination are given in the Appendix A and B, respectively.

## 2. Photometry

### 2.1. Optical

Most of the optical photometry comes from previous  $B$ ,  $V$ ,  $R_C$  and  $I_C$  broad-band imaging observations performed by Alcalá et al. (2004), who obtained CCD mosaic images with the Wide Field Imager (WFI) camera at the ESO/MPIA 2.2m telescope (La Silla Observatory, Chile, program No. 64.I-0355), covering a sky-area of about  $36' \times 34'$  around NGC 1788. The pre-reduction of the raw images, as well as the astrometric and photometric

calibration have been already discussed in Alcalá et al. (2004). In order to improve the photometry of the blended sources, we carried out point spread function fitting photometry on the images using the DAOPHOT package (Stetson 1987) under the IRAF<sup>1</sup> environment.

Further photometric observations of six previously known members of L1615/L1616 (Alcalá et al. 2004), still lacking optical photometry and falling outside the sky-area covered by WFI, were carried out in November 17th and 18th, 2006 with the 91 cm telescope at Catania Astrophysical Observatory (OAC). The observations were performed in the Johnson *UBV* standard system under photometric sky conditions, by using a photon-counting single-head photometer equipped with an EMI 9893QA/350 photomultiplier. In order to determine the transformation coefficients to the Johnson standard system, several standard stars selected from the General Catalogue of Photometric Data (GCPD, Mermilliod et al. 1997) and from Landolt (1992) were also observed in between the targets observations. The observing set-up and the data reduction were the standard ones already adopted during previous observational campaigns of low-mass stars (see, e.g., Marilli et al. 2007).

## 2.2. Near-infrared

Near-infrared *J*, *H* and *Ks* photometry of a  $\sim 30' \times 30'$  region centered on NGC 1788 was obtained using the SOFI camera at the ESO NTT telescope (program No. 70.C-0629) on December 17th, 2002 and January 16th, 2003. 36 pointings of the  $5' \times 5'$  field of view were required to cover the field in each band. Several dithered exposures were obtained for a total integration time per pointing of 80 seconds in the *J* band and 180 seconds in the *H* and *Ks* bands. The data were corrected for electronic crosstalk, differential flat fielding, and illumination following standard SOFI procedures under IRAF.

Photometric calibration was obtained observing a set of standard stars from the list of Persson et al. (1998) (Las Campanas Observatory standards). Source extraction and aperture photometry were performed using the SExtractor software package (Bertin & Arnouts 1996); aperture corrections were estimated from sources away from crowded regions and applied to all extracted sources. The limiting magnitudes at  $3\sigma$  level achieved in our survey are 19, 18 and 17.5 mag at *J*, *H*, and *Ks*, respectively.

---

<sup>1</sup>IRAF is distributed by the National Optical Astronomy Observatory, which is operated by the Association of the Universities for Research in Astronomy, inc. (AURA) under cooperative agreement with the National Science Foundation.

### 3. Spectroscopy

Based on  $I_C$  versus  $(R_C - I_C)$  colour-magnitude diagram and theoretical isochrones from Baraffe et al. (1998), Alcalá et al. (2004) selected a sample of about 200 PMS star and BD candidates in L1615/L1616, by using the spectroscopically confirmed young low-mass stars to define the PMS locus, as shown in their Figure 12. In addition to this sample, 8 X-ray emitting stars detected by the ROSAT All-Sky Survey (RASS), as well as mid-infrared sources (Stanke et al. 2002) and  $H\alpha$  emission-line objects (Nakano et al. 1995), were also selected as further PMS star candidates by Alcalá et al. (2004). We performed the spectroscopic follow-up of about 70 % of the candidates in this sample, down to  $I_C \approx 19$  mag, in order to definitively assess their nature and single out the young objects. Additionally, about 30 % of field stars with  $I_C \lesssim 20.0$  mag was also observed in order to detect possible “veiled” PMS stars which might have escaped the selection criterion (see later Figure 8).

Intermediate- and low-resolution spectra were acquired during different runs at the ESO Very Large Telescope (VLT; Paranal Observatory, Chile), by using the FOcal Reducer and low-dispersion Spectrograph 2 (FORS2; Appenzeller et al. 1998) and the VISible Multi-Object Spectrograph (VIMOS; LeFevre et al. 2003). Multi-object intermediate-resolution spectroscopy was also performed with the Fibre Large Area Multi-Element Spectrograph (FLAMES; Pasquini et al. 2002), but these observations will be described in more detail in a forthcoming paper. The journal of the FORS2 and VIMOS observations is given in Table 1. The distribution on the sky of the area covered by the FORS2, VIMOS, and FLAMES spectroscopic follow-ups is shown in Figure 1. In the following sub-sections a brief description of the spectroscopic observations and data reduction is presented.

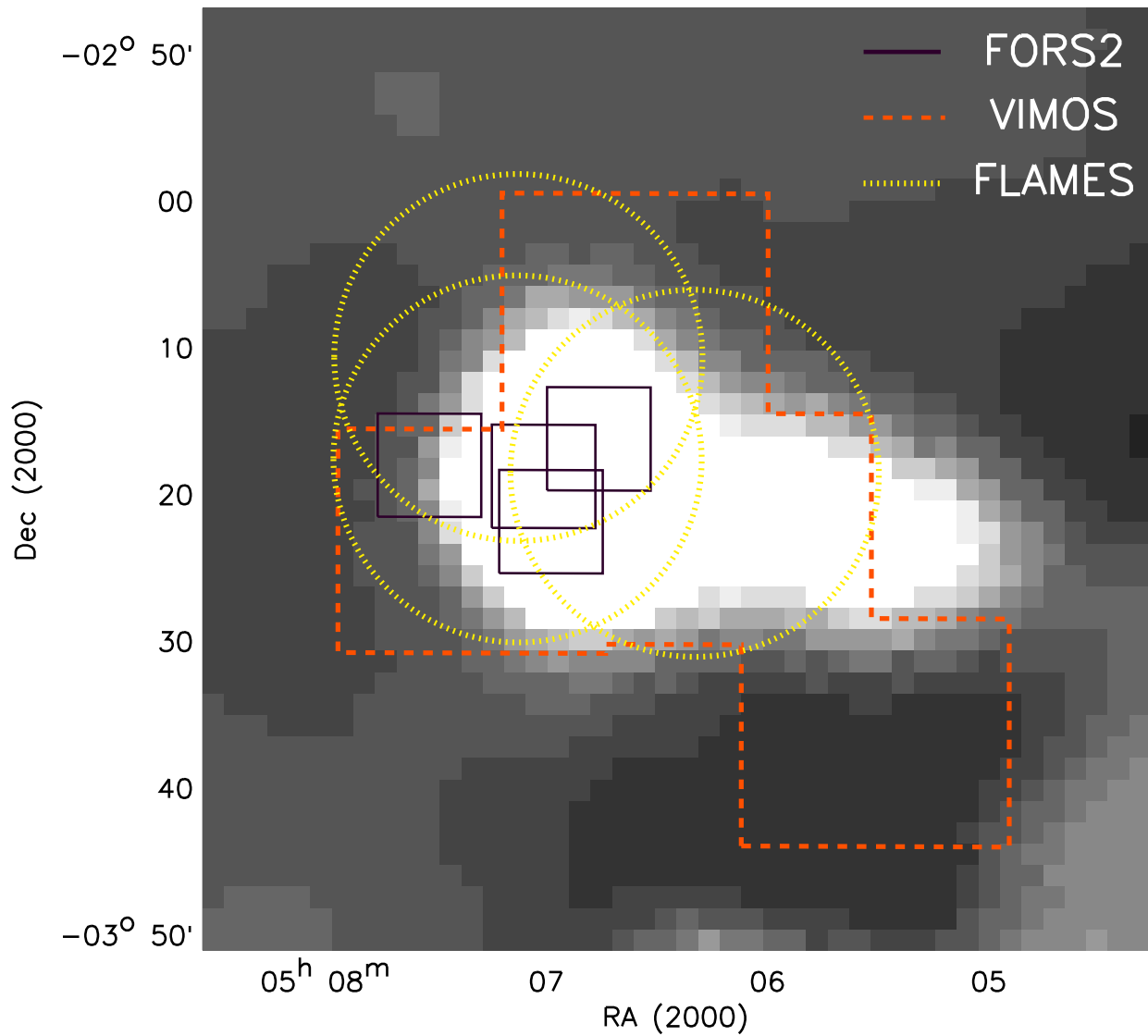


Fig. 1.— Sky areas surveyed by the FORS2 (continuous lines), VIMOS (dashed lines), and FLAMES (dotted lines) spectroscopic follow-ups overlaid on the IRAS 100  $\mu\text{m}$  dust emission map covering a sky-area of about  $1^\circ \times 1^\circ$  around L1615/L1616. Note that the gaps of about  $2'$  between the four VIMOS quadrants are not reproduced in the figure.

### 3.1. FORS2 observations

Intermediate-resolution ( $\lambda/\Delta\lambda=2140$ ) FORS2 spectra of the PMS candidates mainly projected on the NGC 1788 reflection nebula were collected in service mode (ESO program No. 70.C-0536) on the nights 7, 22, 25 February and 8 March 2003, under mostly clear and stable weather conditions, with seeing typically in the range  $0''.8 - 1''.0$ . These observations were performed setting the spectrograph in the multi-object spectroscopy mode. A total of 5 mask configurations, each including 18–19 objects, were observed. Three consecutive spectra of 960 sec were obtained for each mask configuration in order to remove cosmic-ray hits and improve the signal to noise (S/N) ratio. Bias, flat-spectrum lamp, and Ar/He/Ne lamp exposures for each mask were taken in daytime according to the FORS2 standard calibration plan. The typical S/N ratio for a  $I_C \approx 16$  mag star was on the order of 90.

The standard data reduction process was carried out with a semi-automatic pipeline that we have developed on the basis of both MIDAS<sup>2</sup> (Warmels 1991) and IRAF package. The reduction includes bias subtraction, flat-field division, wavelength calibration, sky subtraction and one-dimensional spectra extraction. Relative flux calibration was achieved observing five spectrophotometric standard stars from Hamuy et al. (1992, 1994).

### 3.2. VIMOS observations

The VIMOS observations were performed in service mode (ESO program No. 074.C-0111) during the period from 9 December 2004 to 12 March 2005. The weather conditions were photometric with seeing varying between  $0''.6$  and  $1''.2$ . The larger sky-area covered with VIMOS allowed us to extend the spectroscopic survey in a wider region around the NGC 1788 reflection nebula<sup>3</sup>. Furthermore, we carried out both intermediate- ( $\lambda/\Delta\lambda=2500$ ) and low-resolution ( $\lambda/\Delta\lambda=580$ ) spectroscopy, in order to detect the Li I  $\lambda 6708$  Å absorption line and measure its equivalent width, as well as to obtain a wider wavelength range for spectral type classification purpose (see Section 5.2).

A total of 3 intermediate- and 6 low-resolution mask configurations, each including an average number of about 100 targets, were observed. To efficiently pursue our programme and maximise the number of observed fields, only one exposure of 900 sec and one of 2000 sec were obtained for each low- and intermediate-resolution mask configuration, respectively.

---

<sup>2</sup>MIDAS is developed and maintained by ESO.

<sup>3</sup>Note, however, that the gaps of about  $2'$  between the four VIMOS quadrants prevented us from performing a uniform coverage.

The typical S/N ratio at  $I_C \approx 16$  mag was about 80 and 180 for the intermediate- and low-resolution spectra, respectively.

Five spectrophotometric standard stars from Oke (1990) and Hamuy et al. (1992, 1994) were observed to perform the absolute flux calibrations. Bias and flat field frames as well as wavelength calibration exposures were acquired during daytime, following the service mode VIMOS calibration plan.

The VIMOS spectra were automatically reduced by using the ESO pipeline, full details of which are given by Izzo et al. (2004). In order to check the reliability of the data reduction, the spectra were also independently processed by using the VIMOS Interactive Pipeline Graphical Interface (VIPGI; Scodreggio et al. 2005), obtaining consistent results.

### 3.3. FLAMES-GIRAFFE observations

The FLAMES-GIRAFFE observations were performed in visitor mode (ESO program No. 076.C-0385) during the nights 28 February 2006 and 1, 2 March 2006, under good seeing conditions ( $0''.7 - 1''.0$ ), setting the spectrograph in the MEDUSA configuration. The low-resolution grating LR06 was used in conjunction with an order separating filter and a slit width of  $1''$ . The adopted configuration yielded a spectral coverage of about  $750 \text{ \AA}$  ( $6438\text{--}7184 \text{ \AA}$ ) with a mean resolving power  $\lambda/\Delta\lambda=8600$ .

Since these observations are part of a separate study on radial velocities in L1615/L1616, these data will be described in more detail in a future paper. Here we have used the FLAMES spectra of only three objects, namely TTS 050644.4–032913, RX J0507.3–0326, and TTS 050741.0–032253 (see Table 2), for which both FORS2 and VIMOS observations are missing.

## 4. PMS objects in L1615/L1616

Since lithium is rapidly destroyed in the convective layers of low-mass stars in the early phases of their stellar evolution (Bodenheimer 1965), the presence of strong Li I  $\lambda 6708 \text{ \AA}$  absorption line has been considered as the primary criterion for definitely assessing the PMS nature of the observed stars. The  $H\alpha$  emission has been used as further indicator of youth, though its presence alone does not guarantee the PMS nature of the observed object. Therefore, all the K and M stars with  $H\alpha$  in emission but lacking the Li I absorption line have been rejected and classified as older dKe and dMe field stars projected onto L1615/L1616.



In addition to the above criteria, the presence of forbidden emission lines, as well as non-photospheric UV and infrared continuum excesses (as evidence of bipolar jets, accretion columns, and circumstellar disk, respectively) have yielded further arguments on the PMS nature of the young stars identified in L1615/L1616.

Based on these criteria, we have identified 25 new PMS stars with spectral type later than about K1. By adding these sources to the previously reported PMS objects (Alcalá et al. 2004), the number of optically detected young stars known so far in L1615/L1616 rises to 56 objects<sup>4</sup>. The full sample is listed in Table 2; coordinates are those from the 2 Micron All Sky Survey (2MASS; Cutri et al. 2003) point source catalogue, which have a precision of about 0".1. All the PMS stars revealed by our spectroscopic follow-up, but not detected in previous X-ray and H $\alpha$  surveys, have been designated with “TTS” followed by their position, according to the IAU convention. By adding the millimeter Class-0 protostar discovered by Stanke et al. (2002), which is not reported in Table 2, the young population of L1615/L1616 increases to 57. Thus, our spectroscopic survey almost has doubled the number of confirmed PMS objects associated to L1615/L1616. Some examples of FORS2 and VIMOS spectra are shown in Figure 2.

In total, 4 out of the 8 X-ray emitting sources listed by Alcalá et al. (2004), namely RX J0506.8–0305, RX J0507.4–0317, RX J0507.6–0318, and RX J0507.3–0326, have been spectroscopically confirmed as PMS stars; the other X-ray sources (RX J0506.5–0320, RX J0506.4–0323, RX J0506.4–0328W, and RX J0506.4–0328E) turned out to be field active stars. Note that lithium has been detected for the first time in the spectrum of the mid-infrared source L1616 MIR4 (Stanke et al. 2002).

The S/N ratio of the spectra of the faint sources TTS 050654.5–032046 and TTS 050730.9–031846 turned out to be insufficient for a reliable measurement of their Li I equivalent width. Nevertheless, the presence of a broad and strong H $\alpha$  emission in both spectra (Table 4) can not be explained by chromospheric activity only and is typical of classical T Tauri stars. Indeed, according to the definition by White & Basri (2003), the upper limit on the H $\alpha$  equivalent width for chromospheric activity, in the spectral range M3–M5.5, is 40 Å. TTS 050654.5–032046 and TTS 050730.9–031846 have spectral type M4 and M5.5 and equivalent width 60 Å and 290 Å, respectively; thus, they are clearly accretors.

The star Kiso A-0974 17 was first classified as a H $\alpha$  emission-line object by Nakano et al. (1995). Although Alcalá et al. (2004) did not obtain any spectrum of this source, they included it in their list of PMS stars. We observed this object during the FLAMES spectro-

---

<sup>4</sup>Note that the star Kiso A-0974 17 (Nakano et al. 1995; Alcalá et al. 2004) has been excluded from our list of PMS objects (see below).

scopic run. Neither  $H\alpha$  emission nor Li I absorption line were observed in its spectrum. This could be due to a mismatch between the  $H\alpha$  emission source and the optical counterpart detected by Nakano et al. (1995). Thus we excluded this object from our list of PMS stars.

The optical ( $UBVR_CI_C$ ) and near-infrared ( $JHKs$ ) magnitudes of the 56 optically confirmed PMS stars in L1615/L1616 is presented in Table 3. Some of the objects lack WFI, OAC, and/or SOFI photometry because they fall outside the sky-area covered by our survey, are saturated in our images or are too faint to be observed with the 91 cm telescope at the OAC observatory. Nevertheless, for these stars we retrieved  $I_C$  magnitudes from the TASS Mark IV photometric survey (Droege et al. 2006),  $I_CJ$  magnitudes from the DEep Near-Infrared Survey (DENIS; Epchtein et al. 1997), and  $JHKs$  photometry from the 2MASS point source catalogue. Both the SOFI and DENIS NIR magnitudes were homogenised to the 2MASS photometric system using the transformation equations provided by Carpenter (2001). For a few sources, we used the optical photometry from the literature (Lee 1968; Mundt & Bastian 1980; Taylor et al. 1989; Alcalá et al. 1996; Cieslinski et al. 1997; Frasca et al. 2003; Vieira et al. 2003) as explained in the footnotes of Table 3.

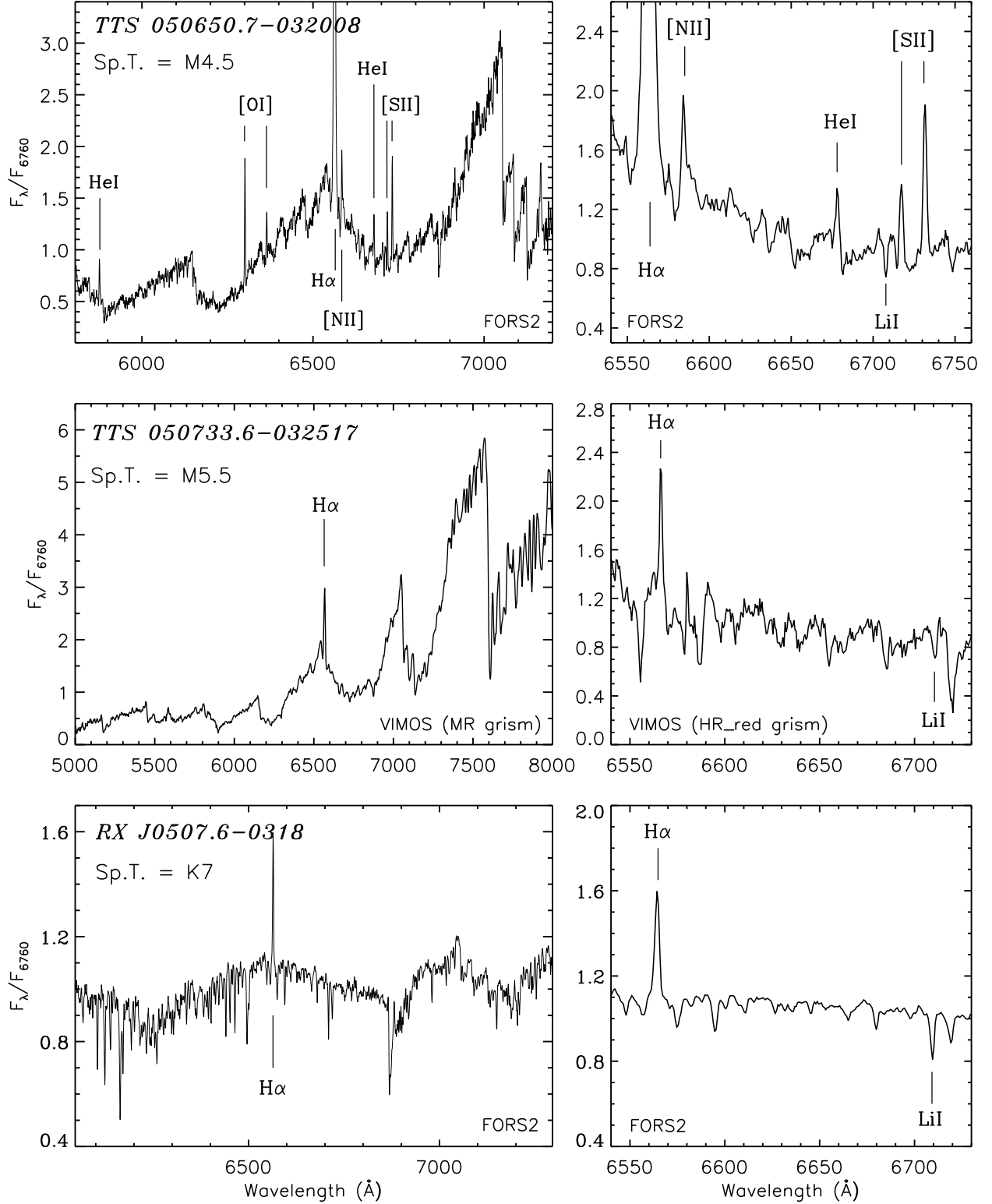


Fig. 2.— VIMOS and FORS2 spectra of three PMS objects in L1615/L1616, namely TTS 050650.7-032008, TTS 050733.6-032517, and RX J0507.6-0318. The spectra have been arbitrarily normalised to the flux at 6760 Å. For each object the whole observed spectrum is shown in the left panel. The spectral range encompassing the H $\alpha$  and Li I  $\lambda$ 6708 Å lines is plotted in more detail in the right panel.

## 5. Data analysis

### 5.1. $H\alpha$ and Li I equivalent widths

$H\alpha$  and Li I  $\lambda 6708$  Å line equivalent widths,  $W(H\alpha)$  and  $W(\text{Li})$ , respectively, were determined by direct integration of the line profiles, as described in Alcalá et al. (2004) and Spezzi et al. (2008), adopting the convention that a negative equivalent width means an emission line. The main source of error on these measurements comes from the uncertainty in the placement of the photospheric continuum, especially for stars later than M1, whose spectra are strongly affected by molecular absorption bands.  $W(H\alpha)$  and  $W(\text{Li})$  for the L1615/L1616 members are reported in the third and fourth columns of Table 4, respectively.

According to the intensity of the  $H\alpha$  emission line and the definitions by White & Basri (2003), we assigned the classical (CTTS) or weak (WTTS) T Tauri star classification to the PMS objects in L1615/L1616 (Table 4).

The additional emission lines observed in the spectra, including the lines of He I  $\lambda 5876$ ,  $\lambda 6678.7$  and  $\lambda 7065.2$  Å, and Na I  $\lambda 5889.9$  and  $\lambda 5895.9$  Å, as well as the forbidden lines of [N II]  $\lambda 6583.5$  Å, [O I]  $\lambda 6300.3$  and  $\lambda 6363.8$  Å, and [S II]  $\lambda 6716.4$  and  $\lambda 6730.8$  Å, are also reported in Table 4. Note that almost only those PMS stars classified as CTTSs show forbidden emission lines in their spectra.

### 5.2. Spectral types and effective temperatures

Spectral types were determined using a modified version of ROTFIT, a code for spectral type and  $v \sin i$  determination developed by Frasca et al. (2003, 2006) under the IDL<sup>5</sup> environment. The general idea of the method, already adopted in Alcalá et al. (2006) and Spezzi et al. (2008), is to recover the spectral type of a star by comparing its spectrum with a suitable grid of templates, taking into account the amount of extinction along the line of sight. Since our spectra are flux calibrated, the method allowed us to get a rough estimate of the extinction ( $A_V$ ) along the line of sight to the star.

To this aim, a library of relative flux calibrated and extinction-corrected templates, with a wavelength coverage encompassing that of the observed spectra, is needed. A suitable grid of intermediate-resolution ( $R \approx 1000 - 5000$ ) templates has been obtained by collecting spectra of dwarf and giant stars from the libraries provided by Martín et al. (1999), Hawley et al.

---

<sup>5</sup>IDL is distributed by ITT Visual Information Solutions, Boulder, Colorado.

(2002), Le Borgne et al. (2003), Valdes et al. (2004), and Bochanski et al. (2007).

In performing the spectral type classification, we first took into account the PMS nature of the stars we were dealing with. Due to the presence of TiO and VO absorption bands which are strongly sensitive to the surface gravity (Torres-Dodgen & Weaver 1993), most of M-type PMS objects show optical spectroscopic features that can be closely reproduced averaging dwarf and giant spectra with the same spectral type (Luhman 1999; Luhman et al. 2003; Guieu et al. 2006). Though the spectra of G-type and K-type PMS stars have been usually compared with template of normal dwarf stars in several works (e.g. Basri & Batalha 1990), we found that also the late K-type objects in our sample are best represented by using an average of dwarf and giant templates of the same spectral type. Indeed TiO and VO absorption molecular bands are still present in late K-type stars, although they are very weak.

Thus, both late-type dwarf and giant templates were included in our grid of reference spectra; moreover, for spectral types later or equal than K5, we also built up an *ad hoc* grid of templates by averaging dwarf and giant spectra of the same spectral sub-class. Furthermore, starting from spectral types later than K7, we constructed templates for the half sub-classes (e.g. K8.5, M0.5, M1.5, etc.) by averaging the two contiguous spectra. Indeed, the intensity of the absorption molecular bands characterising late-type stars displays a rather strong variation from one spectral sub-class to the other, allowing to appreciate differences of half a sub-class. Some details on the spectra fitting procedure is provided in Appendix A.

The spectral types of the PMS objects in our sample are reported in the second column of Table 4. From an inspection of the residuals of the fitting procedure we have estimated an accuracy of about  $\pm 1$  sub-class for stars earlier than K7 and about  $\pm 0.5$  sub-class for cooler objects. A typical uncertainty on  $A_V$  of  $\pm 0.2$  mag was found. For all the objects observed at least twice, with different spectrographs and/or resolving powers, we obtained consistent results, regardless of spectral resolution and wavelength coverage. For the sake of homogeneity, we re-determined the spectral types also for the previously known low-mass members, by using the spectra from Alcalá et al. (2004). A general agreement within one/two spectral sub-classes was found between our classification and the one reported in the literature (Cohen & Kuhi 1979; Alcalá et al. 2004).

For the two early-type stars HD 293815 and Kiso A-0974 15, we have adopted the spectral types from Sharpless (1952) and Vieira et al. (2003), respectively. Both stars were spectroscopically observed by us, but many photospheric features suitable for an accurate early-type classification were not covered in our spectra. Nevertheless, we attempted a spectral type estimate for both stars by applying the Hernández et al. (2004)’s criteria. The main features we used are the He I  $\lambda 5876$  and  $\lambda 7065.2$  Å absorption lines. The results are consistent with

those reported by Sharpless (1952) and Vieira et al. (2003).

In line with our spectral type classification, the effective temperature ( $T_{\text{eff}}$ ) of each PMS star was assigned on the basis of the following criteria: the dwarf temperature scale from the compilation of Kenyon & Hartmann (1995) was adopted for all the objects with spectral type earlier or equal to K4; for later spectral types an intermediate temperature scale was derived by averaging the giant compilation provided by van Belle et al. (1999) with the dwarf one from Kenyon & Hartmann (1995) for K0-M0 and from Leggett et al. (1996) for M1-M7 spectral types, respectively. The  $T_{\text{eff}}$  values corresponding to the half spectral sub-classes were computed by linear interpolation. The effective temperatures assigned to each PMS object are reported in the second column of Table 5. In assessing the errors on  $T_{\text{eff}}$  the uncertainty on the spectral type classification was taken into account.

### 5.3. Extinction, stellar radii, and luminosities

The method we used for computing extinction, stellar radii, and luminosities follows the general guidelines described in Romaniello et al. (2002, 2006), although we modified their scheme to match our purposes. The eight broad-band magnitudes available for the L1615/L1616 PMS population allowed us to construct the spectral energy distribution (SED) of each PMS star covering a wide spectral range, from optical to near-infrared wavelengths (see Table 6). By using simultaneously all the photospheric colours encompassed by the SED, we computed for each object both the interstellar extinction ( $A_V$ ) and the ratio of total-to-selective extinction ( $R_V = A_V/E_{B-V}$ ), as well as the stellar radius ( $R_*$ ) and luminosity ( $L_*$ ).

Apart for eventual ultraviolet and infrared excesses caused by the presence of an interacting accretion disk around the PMS star and by the related boundary layer, or hot accretion spots, the shape of the observed SED is mostly determined by the effective temperature of the object, the amount of dust along the line of sight, and the dust-grain mean size in the interstellar/circumstellar environment. Therefore, once the effective temperature is known, both the value of  $A_V$  and  $R_V$  may be recovered simultaneously by fitting the observed SED with a grid of theoretical ones. Indeed, both the star radius and distance cause just a rigid shift of the flux on a logarithmic scale, without affecting the shape of the SED. Theoretical SEDs may be obtained by using stellar atmosphere models with the same effective temperature as the star and reddened by various amount of  $A_V$  and  $R_V$ .

A detailed description of the SED fitting procedure is reported in Appendix B. Here we want to stress that, our two-parameter fitting procedure can be applied only to the objects

which are significantly affected by extinction, i.e to the stars which are still deeply embedded in their parent cloud. Indeed, for slightly reddened stars the value of  $A_V$  is relatively insensitive to changes in the slope of the reddening law ( $R_V$ ), as shown in Appendix B. Therefore, for all the objects for which  $A_V$  turned out to be less than about 0.5 mag we reiterated the fitting procedure fixing  $R_V$  to the standard value of 3.1. The same assumption was adopted for all the objects lacking optical photometry and for the veiled star TTS 050649.8–032104.

The values of  $A_V$ ,  $R_V$ ,  $R_*$ , and  $L_*$  are listed in Table 5. For all the objects spectroscopically observed in this work, we found that the value of  $A_V$  derived from the SED fitting procedure is in agreement, within  $\sim 0.2$  mag, with the one obtained from the spectral type classification.

$R_V$  was derived for 15 out of the 56 PMS stars in L1615/L1616 (Table 5). We found a weighted mean value of  $3.32 \pm 0.04$ , closely matching the standard one of 3.1, typical of the diffuse interstellar medium. For the Herbig star Kiso A-0974 15 we obtained a value of  $R_V = 5.5$  (see Table 5). This may be related to the presence of dust grains around the intermediate-mass star which are larger in size than those characteristic of the interstellar medium, as already found by different authors in large samples of HAeBe stars (Thé et al. 1981; Herbst et al. 1982; Waters & Waelkens 1998; Whittet et al. 2001; Hernández et al. 2004).

#### 5.4. Masses and Ages

The mass and age of each member of L1615/L1616 have been derived by comparing the location of the object on the H-R diagram with the theoretical PMS evolutionary tracks by Baraffe et al. (1998) & Chabrier et al. (2000), D’Antona & Mazzitelli (1997), and Palla & Stahler (1999) (Figure 3).

Since stellar evolutionary models are still rather uncertain, particularly in the low-mass star and sub-stellar regimes ( $M < 0.5 M_\odot$ , Baraffe et al. 2002), the use of different evolutionary tracks allowed us to estimate the model-dependent uncertainties associated with the derived stellar parameters.

Table 7 lists masses and ages of the L1615/L1616 members as inferred by the three sets of models. Note that the evolutionary tracks by Baraffe et al. (1998) & Chabrier et al. (2000), D’Antona & Mazzitelli (1997), and Palla & Stahler (1999) are available in the mass range  $0.003 \leq M \leq 1.40 M_\odot$ ,  $0.017 \leq M \leq 3 M_\odot$ , and  $0.1 \leq M \leq 6 M_\odot$ , respectively. Note also that isochrones by Baraffe et al. (1998) & Chabrier et al. (2000) are available only for ages greater or equal than 1 Myr.

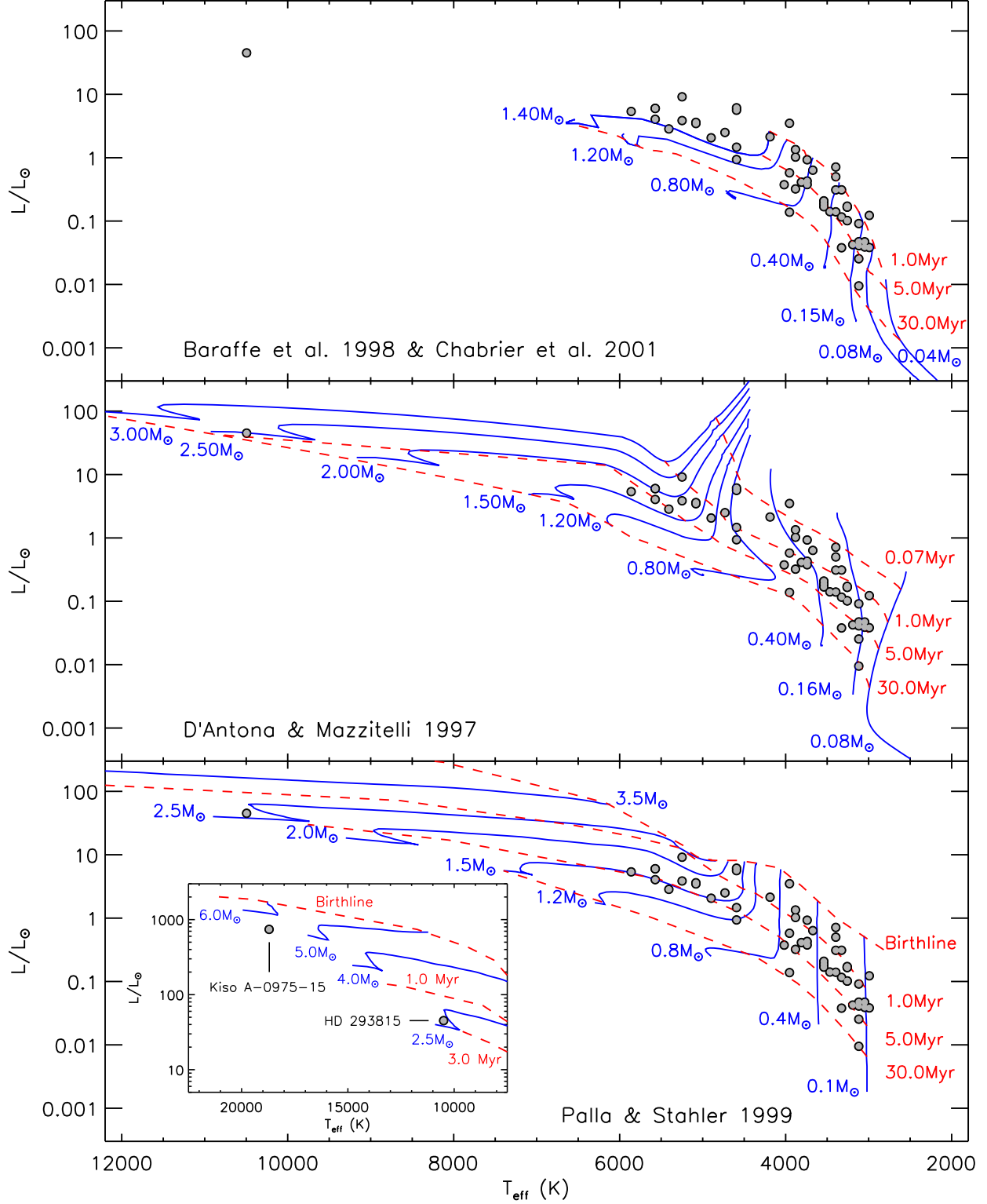


Fig. 3.— H-R diagram for the young population in L1615/L1616; the PMS evolutionary tracks by Baraffe et al. (1998) & Chabrier et al. (2000) (upper panel), D’Antona & Mazzitelli (1997) (central panel), and Palla & Stahler (1999) (lower panel) are over-plotted. The H-R diagram for the intermediate-mass members of L1615/L1616, namely HD 293815 and Kiso A-0974 15, is shown in the inset of the lower panel.



## **6. Discussion**

Once the physical parameters of the PMS objects are known, we can study the star formation in L1615/L1616. In the next sub-sections we discuss the history, rate and efficiency of star formation, and some issues related to the mass-spectrum.

### **6.1. The star formation history**

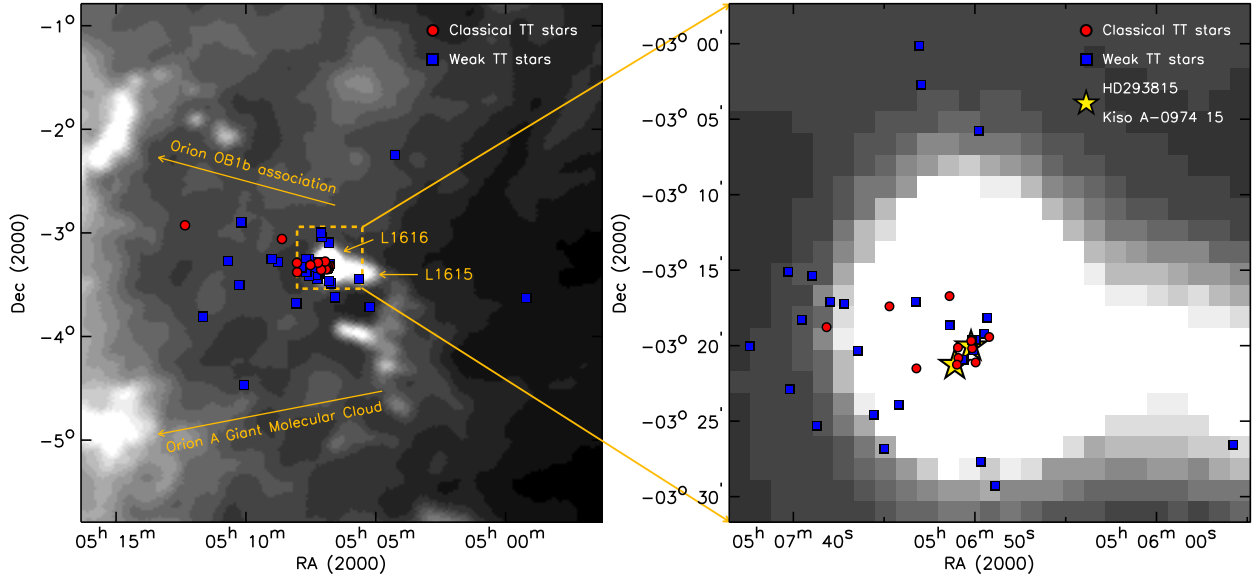


Fig. 4.— IRAS 100 $\mu$ m dust emission map covering a sky-area of  $5^\circ \times 5^\circ$  around L1615/L1616 (left panel). The Classical and Weak T Tauri stars are represented with filled dots and squares, respectively. The upper arrow shows the direction to the Orion OB1 associations, located at about  $7.5^\circ$  ( $\sim 60$  pc at a distance of 450 pc) to the North-East of L1615/L1616. The lower arrow points toward the Orion A Giant Molecular Cloud, also located at about  $7.5^\circ$  to the South-East of L1615/L1616. The dashed square defines the area surveyed with WFI. This region is zoomed in the right panel, where the two intermediate-mass members HD 293815 and Kiso A-0974 15 are marked with five-pointed star symbols.

Based on the most complete census of the L1615/L1616’s population performed in this work, we further investigated the triggered star formation scenario suggested by Ramesh (1995), Stanke et al. (2002), and Alcalá et al. (2004).

In left panel of Figure 4 the IRAS 100  $\mu\text{m}$  dust emission map of a  $5^\circ \times 5^\circ$  sky-area around L1615/L1616 is shown. About 64 % of the CTTSs are clustered, in the densest part of L1615/L1616, i.e. within the boundaries of the NGC 1788 reflection nebula and to the West of the bright rim of the cloud (Figure 4, right panel). Such rim is located to the East of NGC 1788, at  $\sim 6.5'$  from the head of the cometary cloud (about 0.85 pc at a distance of 450 pc) and it is directly exposed to the UV radiation from the Orion OB stars. On the other hand, the WTTSs are more scattered (only  $\sim 22\%$  is projected on NGC 1788) and mainly occupy the side of the cloud facing the OB1 associations and to the East of the bright rim.

By applying the Kolmogorov-Smirnov test to the WTTS and CTTS age distributions we found that the two populations are similar at a confidence level of  $\sim 80\%$ . Thus, it seems there are no age differences between CTTSs and WTTSs in our PMS sample. This result is consistent with previous PMS populations studies (see Feigelson & Montmerle 1999, and reference therein); CTTSs are predicted to have ages between about 0.5 and 3 Myr, although some stars retain CTTS characteristics even at ages as old as 20 Myr. On the other hand, many WTTSs occupy the same region on the H-R diagram as CTTSs do, whereas some of them are approaching the zero-age main sequence.

The age distribution of the L1615/L1616 population peaks between 1 and 3 Myr, depending on the adopted evolutionary tracks (Figure 5, right panels). This is in agreement with the findings by Alcalá et al. (2004), but the age spread found by us is significantly higher than what these authors claim, exceeding the value expected on the basis of the uncertainties on luminosity and temperature. The L1615/L1616 members span a wide range in age, from less than 0.1 Myr up to about 30 Myr. This might suggest multiple events of star formation in the cloud, which would further support the hypothesis of triggered star formation.

In order to investigate a possible age difference between “on-cloud” and “off-cloud” PMS objects, we divided the sample in two groups, fixing as dividing line the bright rim of the cloud. Twenty of 56 objects in our sample are located within the boundaries of NGC 1788, i.e. to the West of the bright rim, while 36 are off-cloud members. The age distributions of the two groups are shown in Figure 6. The on-cloud PMS stars are statistically younger than those located to the East of the bright rim, regardless of the adopted evolutionary tracks. Applying a Kolmogorov-Smirnov test we found that the probability that the two sets are sub-sample of the same statistical population is very low; in particular, we found confidence levels of 1.29, 0.18, and 0.19 % when using the PMS evolutionary tracks by Baraffe et al.

(1998) & Chabrier et al. (2000), D’Antona & Mazzitelli (1997), and Palla & Stahler (1999), respectively. We thus concluded that there is a clear age difference between the two groups of stars.

The above findings further support the scenario of triggered star formation in L1615/L1616, as proposed by Stanke et al. (2002). In this context, the spatial dispersion and older age of the “off-cloud” members can be explained as a consequence of the “rocket acceleration” effect. As recently pointed out by Kun et al. (2004), this acceleration continues after the onset of star formation and the parental cloud is further accelerated with respect to the newly formed objects. As a consequence, the cloud is soon swept off the newly formed stars. This hypothesis, together with the rapid dispersion typical of small clouds, causes the spatial displacement of the oldest cloud members. The conspicuous number of PMS stars found apparently isolated from classical star forming regions (e.g. Alcalá et al. 1995; Covino et al. 1997; Guillout et al. 1998a,b; Frasca et al. 2003; Zickgraf et al. 2005) might be a consequence of this mechanism as well.

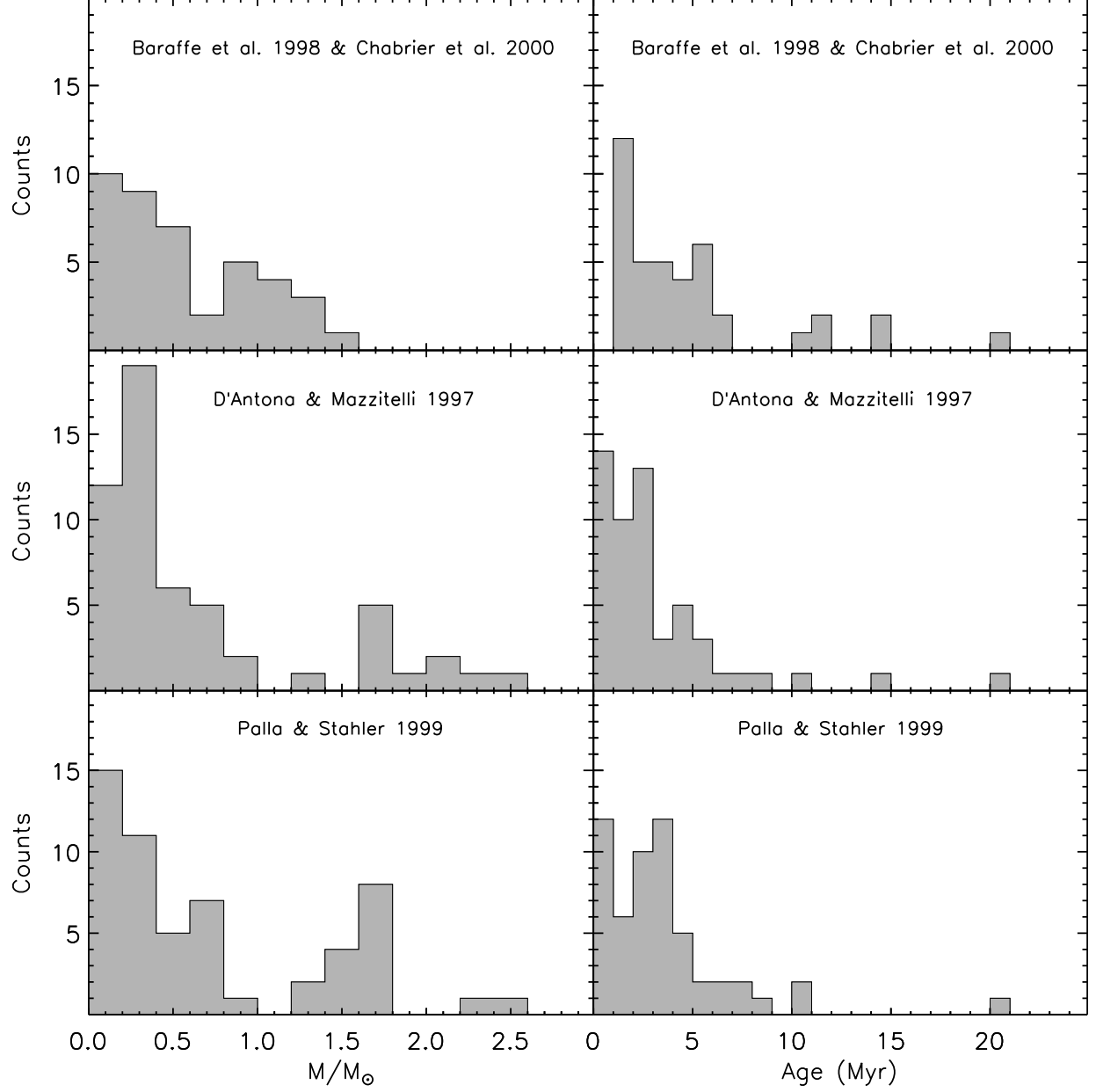


Fig. 5.— Mass (left panel) and age (right panel) distributions of the L1615/L1616 PMS population derived by using the evolutionary tracks by Baraffe et al. (1998) & Chabrier et al. (2000) (upper panels), D’Antona & Mazzitelli (1997) (central panels) and Palla & Stahler (1999) (lower panels).

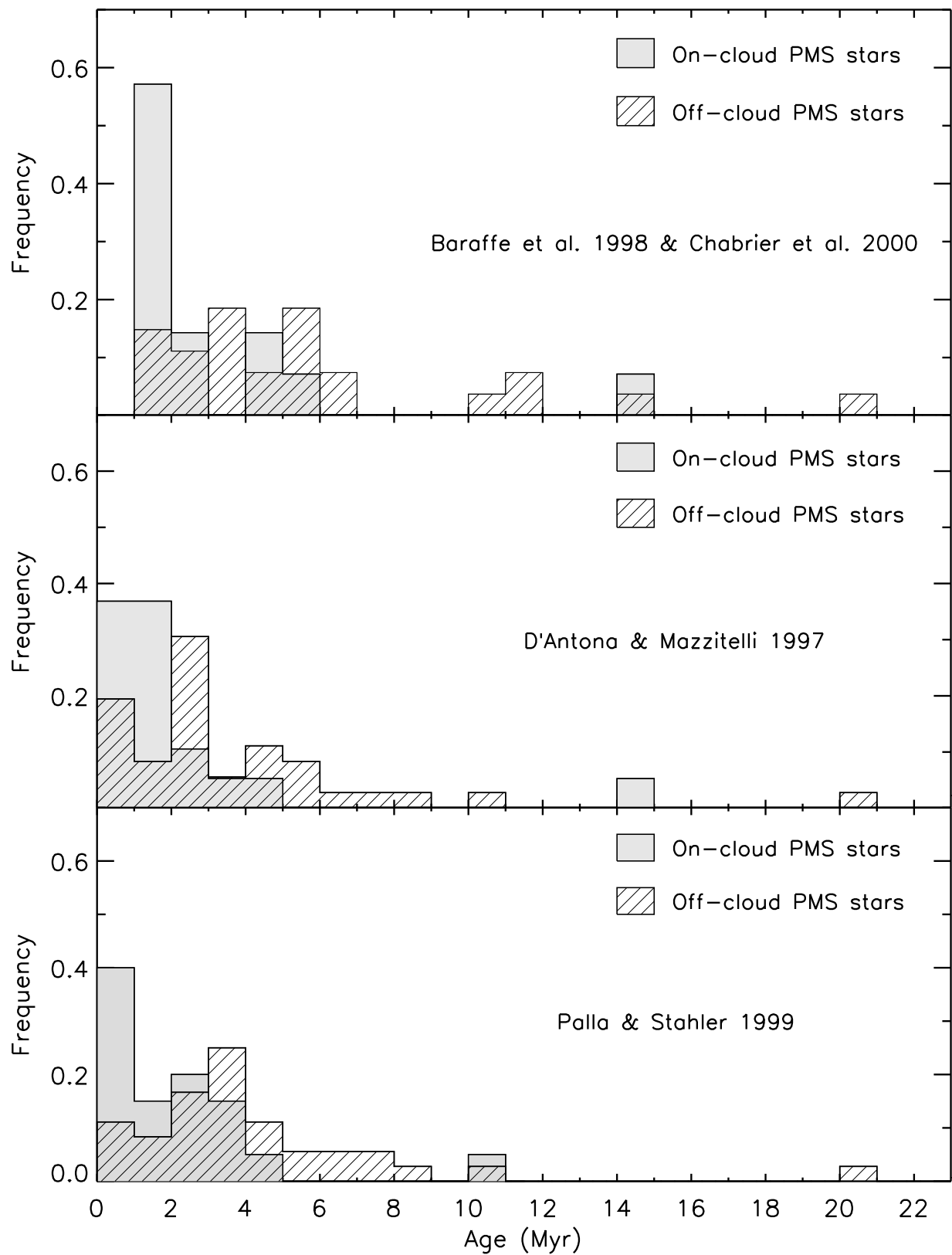


Fig. 6.— Age distributions of the on-cloud and off-cloud PMS stars in L1615/L1616 derived by using the evolutionary tracks by Baraffe et al. (1998) & Chabrier et al. (2000) (upper panel), D'Antona & Mazzitelli (1997) (central panel) and Palla & Stahler (1999) (lower panel).

## 6.2. The star formation efficiency

Based on  $^{12}\text{CO}$  and  $^{13}\text{CO}$  column density maps, Ramesh (1995) estimated that the mass of L1616 alone is in the range  $169 - 193 M_{\odot}$ , depending on the used tracer. Yonekura et al. (1999) mapped both L1615 and L1616 in the CO J=1-0 transition line. They inferred that the mass of the cloud system as a whole is  $\sim 530 M_{\odot}$ ,  $\sim 350 M_{\odot}$  and  $\sim 440 M_{\odot}$  based on  $^{12}\text{CO}$ ,  $^{13}\text{CO}$  and  $^{18}\text{CO}$  observations respectively. They also derived the mass of the  $^{13}\text{CO}$  and  $^{18}\text{CO}$  cores (i.e. L1616 only) finding a value of  $\sim 146 M_{\odot}$  and  $\sim 161 M_{\odot}$ , in good agreement with the Ramesh (1995)’s determination.

Alcalá et al. (2004) estimated the SFE in L1616 to be  $\sim 14\%$ , i.e. higher than the average value measured in other low-mass star forming region ( $\lesssim 3\%$ ). The SFE reported by Alcalá et al. (2004) for L1616 is based on the cloud mass reported by Ramesh (1995) and the total stellar mass of the 32 members of the cloud investigated by the authors (i.e.  $\sim 30 M_{\odot}$ ).

Since the star formation history of L1615 and L1616 is intimately connected, we have re-calculated the SFE considering the system L1615 plus L1616 as a whole. By using the NICER color excess method by Lombardi & Alves (2001), we mapped the dust extinction of the cloud complex and derived its mass. In the NICER technique the  $J - H$  and  $H - K_s$  colours of the field stars are compared to the colours of stars in a nearby reference field. The colour-excesses of the field stars are then combined and transformed to the visual extinction  $A_V$ , fixing the form of the reddening curve. The normal interstellar extinction law derived by (Cardelli et al. 1989) has been adopted by us for this purpose. We retrieved the 2MASS colours of all the point-like sources located in a  $50' \times 50'$  region centered on NGC 1788 and in a reference field close to the L1615/L1616 cloud<sup>6</sup>. The latter field was selected by using the nearby low-intensity regions of the IRAS  $100\mu\text{m}$  dust emission map, according to prescription by Kainulainen et al. (2006). Finally, the visual extinction map resulting from the NICER method was converted to cloud mass by assuming the standard gas-to-dust ratio (Bohlin et al. 1978). We found a value of  $\sim 550 M_{\odot}$ , in good agreement with the one inferred by Yonekura et al. (1999) on the basis of  $^{12}\text{CO}$  observations. Based on this value and on the total mass of the 56 present-day known members of the complex (i.e.  $41\text{--}46 M_{\odot}$ , depending on the adopted evolutionary tracks), we derived a SFE in L1615/L1616 of  $7\text{--}8\%$ , i.e. significantly lower than the previous estimate by Alcalá et al. (2004), but still in good agreement with the one generally found in giant molecular clouds hosting OB associations ( $5\text{--}10\%$ ) and predicted by theoretical calculations on the formation of OB associations (see

---

<sup>6</sup>The SOFI survey is only centered on the densest part of the cloud and can not be used to map the cloud as a whole.

Clark et al. 2005, and reference therein).

### 6.3. Density of star formation and star formation rate

An interesting question is whether L1615/L1615 can be considered as a cluster. According to the definition suggested by Lada & Lada (2003), a cluster is a group of some 35 members with a total mass density larger than  $1.0 \text{ M}_{\odot} \text{ pc}^{-3}$ . To estimate the density of PMS objects in L1615/L1615, we considered the region spectroscopically surveyed by us (Figure 1). This region covers an area of approximately 0.25 square degrees and includes about 40 PMS objects. Assuming a distance of 450 pc, the resulting area is about  $4 \text{ pc}^2$ , which means a surface density of about 10-11 PMS objects per  $\text{pc}^2$  and a volume density on the order of 7 PMS objects per  $\text{pc}^3$ . In the latter calculation we estimated the volume as  $V = 0.752 \times \text{Area}^{1.5}$  (see Jørgensen et al. 2007), assuming a locally spherical distribution of sources. The average mass of the 40 PMS objects, as determined from the results in Section 5.4, is on the order of  $0.7 \text{ M}_{\odot}$ , which implies a volume density of about  $4\text{-}5 \text{ M}_{\odot} \text{ pc}^{-3}$ . Therefore, the group of 40 PMS objects confined in the spectroscopically surveyed area can be considered as a cluster according to the criterion by Lada & Lada (2003).

Now, it is interesting to estimate the rate at which the stars in this small cluster are formed. According to the results of Section 5.4, we estimated that the total mass in PMS objects in that region is on the order of  $41\text{--}46 \text{ M}_{\odot}$ . Therefore, considering the average age of 2 Myr for these objects (see Figure 5), we found that the cometary cloud is turning some  $20\text{--}23 \text{ M}_{\odot}$  into PMS objects every Myr, which is lower than the star formation rate in other clusters like those in Serpens (Harvey et al. 2007), but higher than in other T associations like Chamaeleon II (Alcalá et al. 2007) and Lupus (Merín et al. 2007). Thus we concluded that L1615/L1616 is a small cluster with a moderate star formation rate.

### 6.4. The Initial Mass Function

Though based on a low-number statistics, the first clue on the Initial Mass Function in L1615/L1616 was given by Alcalá et al. (2004). Based on this study, the IMF in this region appears roughly consistent with that of the solar neighbourhood in the mass range  $0.3 < M < 2.5 \text{ M}_{\odot}$  (Miller & Scalo 1979). The authors also found several candidates for young BDs and estimated the expected number of BDs relative to more massive PMS stars in L1615/L1616 to be intermediate between Taurus ( $\sim 13\%$ , Briceño et al. 2002) and the Trapezium cluster ( $\sim 26\%$ , Luhman et al. 2000).



The depth of the spectroscopic survey conducted in this work goes down to  $I_C \approx 19.0$  mag (i.e.  $M \approx 0.03 - 0.05 M_\odot$ , see Section 6.5), leading to the discovery of young objects with a mass close to the Hydrogen burning limit. We have thus attempted a fair IMF determination down to the low-mass stellar regime (i.e.  $M \gtrsim 0.1 M_\odot$ ).

All the present-day known members of L1615/L1616 have masses in the range between  $\sim 0.1$  and  $5.5 M_\odot$ ; their mean mass varies between  $0.6$  and  $0.8 M_\odot$  depending on the adopted evolutionary tracks (see Table 7 and Fig 5, left panels). However, although our survey recovers most of the previously known young objects in L1615/L1616, the completeness of our PMS sample is different from the one of Alcalá et al. (2004) sample. The latter includes bright and solar-like objects located in areas not covered by the deeper WFI survey. Therefore, we restricted our IMF analysis to the sample of objects that lie on the sky-area covered with WFI (Figure 4, right panel).

The shape of the IMF in the cloud may then be constrained using the usual approximation for the low-mass function ( $\frac{dN}{dM} \propto M^{-\alpha}$ ), as reported by (Moraux et al. 2003). We divided the mass range into mass bins of about  $0.2 M_\odot$ ; this value is larger than the accuracy on mass estimates as derived from the uncertainties on temperatures and luminosities and, at the same time, allows us to have a statistically significant number of objects in each bin.

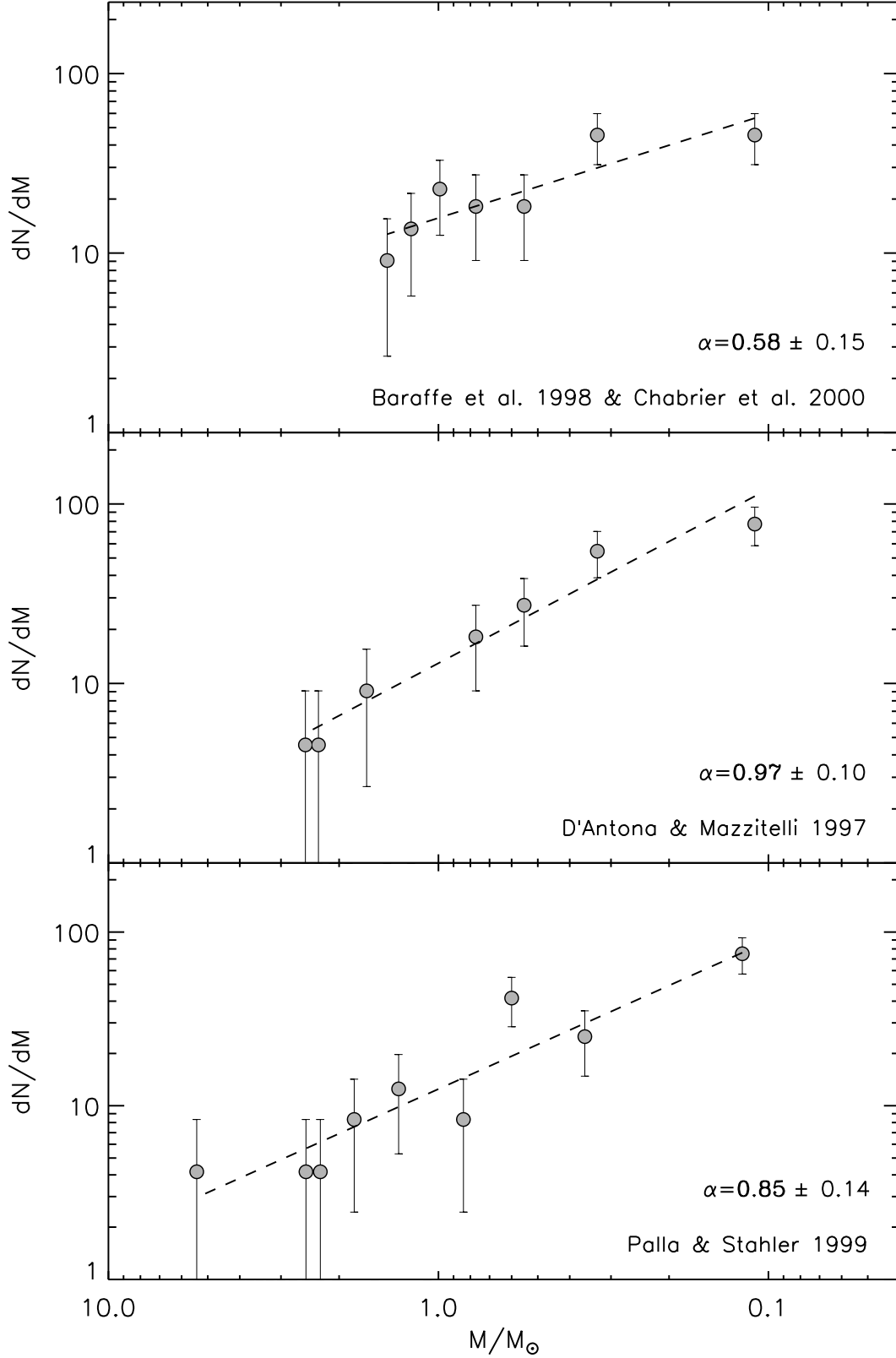


Fig. 7.— The L1615/L1616 IMF between 0.1 and 5.5  $M_\odot$  as derived by using the evolutionary tracks by Baraffe et al. (1998) & Chabrier et al. (2000) (upper panel), D'Antona & Mazzitelli (1997) (central panel) and Palla & Stahler (1999) (lower panel).

Figure 7 shows the IMF in L1615/L1616 as obtained by using the three sets of evolutionary tracks by Baraffe et al. (1998) & Chabrier et al. (2000), D’Antona & Mazzitelli (1997) and Palla & Stahler (1999). Values of  $\alpha$  in the three cases agree within the errors and we can derive a weighted mean value of:

$$\alpha = 0.84 \pm 0.07$$

as the best approximation of the IMF slope in L1615/L1616 in the mass range  $0.1 \leq M \leq 5.5 M_{\odot}$ . We notice, however, that the evolutionary models by D’Antona & Mazzitelli (1997) tend to produce a steeper IMF with respect to those by Baraffe et al. (1998) & Chabrier et al. (2000) and Palla & Stahler (1999), as already found by Spezzi et al. (2008).

In Table 8 the  $\alpha$  slope obtained for the IMF in L1615/L1616 is compared with those obtained in other star forming regions with different ages and environmental conditions. These values indicate a common shape of IMF in the mass range from  $\sim 0.1$  to  $\sim 1 M_{\odot}$ . This provides further evidence of a universal IMF also in the low-mass regime and is in agreement with the results already established for the intermediate and massive star domains (Kroupa 2002).

### 6.5. No sub-stellar objects in L1615/L1616 ?

Prior to our survey, no confirmed BDs in L1615/L1616 were reported in the literature. However, Alcalá et al. (2004) photometrically selected some 30–40 candidates for BDs in this region and estimated a fraction of sub-stellar objects relative to PMS stars ( $R_{SS}$ ) in the range from 18 % to 25 %, i.e. similar to the value measured in the Trapezium cluster (Hillenbrand & Carpenter 2000; Briceño et al. 2002; Muench et al. 2002) and in other OB associations.

Our spectroscopic observations, which investigated about 50 % of the BD candidates with  $I_C \lesssim 19.0$  mag reported by Alcalá et al. (2004), revealed 3–4 young objects with mass  $M \leq 0.1 M_{\odot}$  (see Table 7), close to the Hydrogen burning limit, and no objects with lower mass. However, taking into account the accuracy with which we estimated the masses, these objects could be BDs with a mass just below the Hydrogen burning limit. The  $R_{SS}$  in the cloud would be then around 5–7 %. Though the very low-mass BDs ( $M \lesssim 0.03 M_{\odot}$ ) and some deeply embedded low-mass objects might have escaped detection in our survey, this value should be slightly lower than the one estimated for other T associations (12–15 %; Briceño et al. 2002; López Martí et al. 2004).

The photometric survey conducted by us in L1615/L1616 is spatially and photometrically complete down to  $I_C \approx 21.5$  mag at  $10 \sigma$  level. However, only objects brighter than

$I_C \approx 19.0$  mag could be observed spectroscopically with a S/N ratio sufficient for spectral type classification purpose. A 1–3 Myr old object (i.e. the typical age of the L1615/L1616 population) at the distance of 450 pc (i.e. a distance modulus of 8.27 mag) with a mass  $M \gtrsim 0.03 M_\odot$  would have  $I_C \lesssim 19.0$  mag in the absence of extinction (Baraffe et al. 1998). Thus, in the off-cloud regions of L1615/L1616, where  $A_V \approx 0$  mag, our survey is sensitive down to  $\sim 0.03 M_\odot$ . The visual extinction occurring in the dense head of the cloud varies in the range 1–5 mag which displaces the limiting mass of the objects with  $I_C \lesssim 19.0$  mag to 0.05–0.50  $M_\odot$  (Baraffe et al. 1998). We conclude that we are probably missing the very low-mass objects only in the small dense core of the cloud. Given the peculiar star formation history in this cloud (Section 6.1), the knowledge of its sub-stellar mass spectrum could give crucial insights into the process forming BDs under particular environmental conditions.

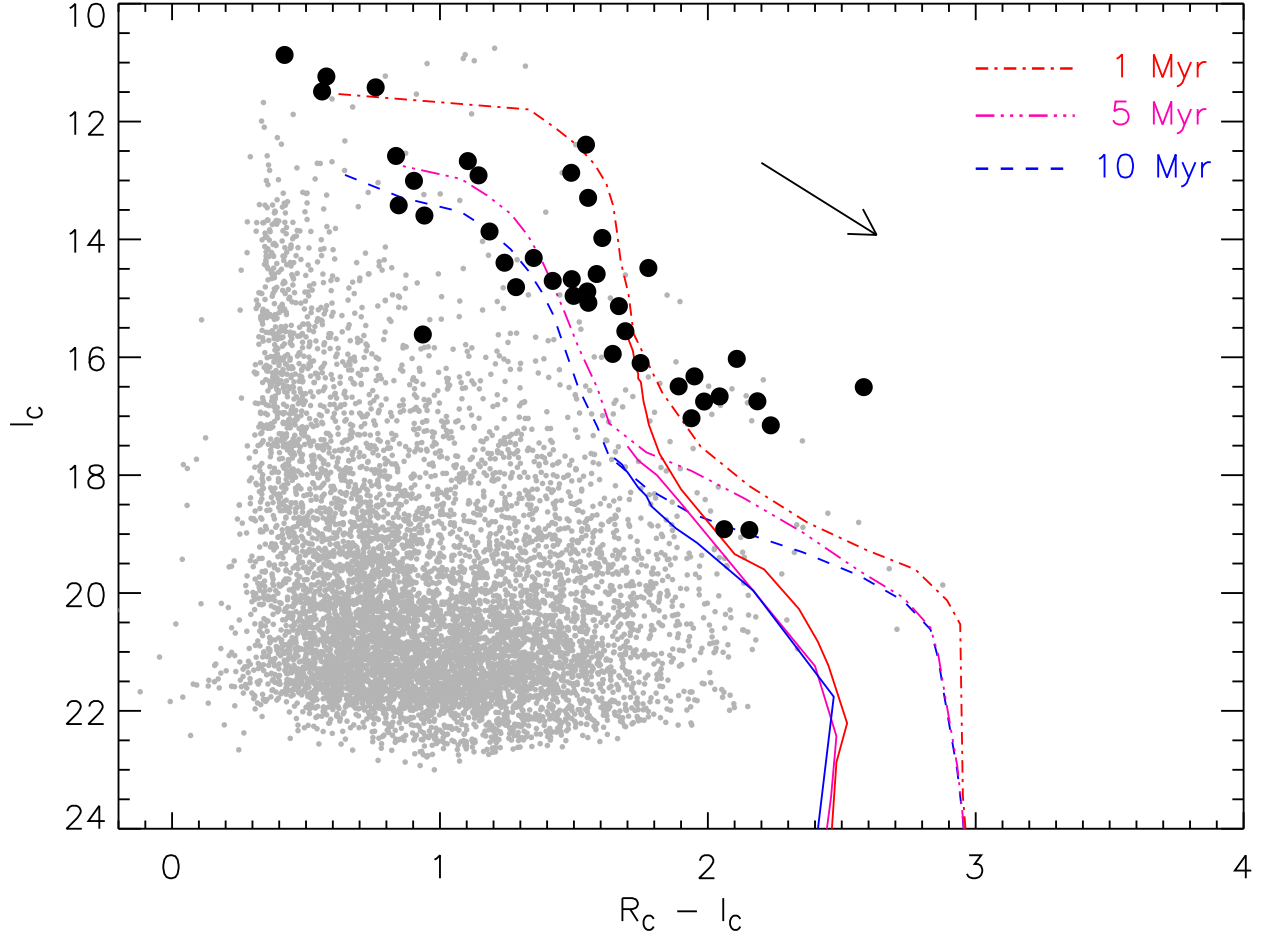


Fig. 8.—  $I_C$  versus  $(R_C - I_C)$  diagram for the point-like objects in L1615/L1616 detected in our WFI survey above  $3\sigma$  level (grey little dots). The theoretical isochrones by Baraffe et al. (1998) & Chabrier et al. (2000) for the Cousins photometric system of Bessel (continuous line) and for the WFI-Cousins system (dashed lines, Spezzi et al. 2007) are overplotted. The PMS stars with both  $R_C$ - and  $I_C$ -band measurements (see Table 3) are overplotted with black big dots. The  $A_V = 2$  mag reddening vector is also shown. The confirmed PMS object falling well below the 10 Myr isochrone is the veiled star TTS 050649.8–032104

The BD candidates sample by Alcalá et al. (2004) was selected by inspection of  $I_C$  versus  $(R_C - I_C)$  colour-magnitude diagram in comparison with the theoretical isochrones by Baraffe et al. (1998) & Chabrier et al. (2000). This approach to search for PMS star and young BD candidates is the most direct way to tackle the problem using optical photometric data; however, in order to select cluster members on the basis of their magnitudes and colours, isochrones that adequately model the data must be used, since the shape of the isochrones may vary significantly from one photometric system to another. The theoretical isochrones for low-mass stars and BDs are provided by Baraffe et al. (1998) & Chabrier et al. (2000) in the Cousins photometric system (Cousins 1976), while the observations by Alcalá et al. (2004) were performed by using the WFI camera at the ESO 2.2m telescope. The WFI filters transmission curves are somewhat different from the original Cousins ones, in particular for the  $I$ -band. Spezzi et al. (2007) have computed *ad hoc* isochrones for the WFI-Cousins system. In Figure 8 these isochrones are compared with those by Baraffe et al. (1998) & Chabrier et al. (2000). The two sets of isochrones appear significantly different, in particular for the coolest objects, i.e.  $(R_C - I_C) > 1.7$ , where the use of the isochrones in the Cousins system would produced many spurious member candidates. This consideration, together with the contamination by background/foreground stars in the field taken into account by the authors, could explain why Alcalá et al. (2004) overestimated the number of BD candidates. The use of the adequate isochrones for the WFI-Cousins system would produce much less BD candidates, in agreement with the number of PMS objects with mass close to the Hydrogen burning limit confirmed by our spectroscopic follow-up (see Table 7).

Though the  $R_{SS}$  estimated by us for L1615/L1616 needs further refinements, the region seems to be poor of BDs, with a  $R_{SS}$  ratio close to that observed in T associations or, perhaps, even lower. Though in L1615/L1616 the radiation from the massive stars in the Orion OB1 associations is likely responsible for the star formation (Section 6.1), this primordial process does not seems to favour the formation of BDs. As reported in Alcalá et al. (2004), the radial velocity (RV) distribution of the stars in L1615/L1616 shows a well defined peak at 22.3 Km/s with the standard deviation of 4.6 Km/s which is consistent with the average RV error (i.e.  $\sim 5$  Km/s). This may indicate that the velocity dispersion of the stars must be less than 5 Km/s. Considering a velocity dispersion of a few Km/s, 2 Myr old objects would disperse over a distance of about 2 pc, which is the approximate projected size of the head of the cometary cloud and has been completely covered by our photometric and spectroscopic observations.

Thus, the results of our study in L1615/L1616 does not play in favour of dynamical ejection or photoevaporation by ionising radiation from massive stars being triggering factors of the BDs formation mechanism.

## 7. Summary

We have undertaken a study of the star formation process in the L1615/L1616 cometary cloud, a small star forming region located in the outskirts of the Orion OB associations. We aimed at characterising its PMS population and studying both its IMF and star formation history, in order to assess the role of the triggered star formation scenario.

Our study is based on optical and near-infrared photometric observations, as well as multi-object follow-up spectroscopy, both carried out using ESO and OAC facilities. Complementary *JHKs* photometric data from the 2MASS and DENIS surveys has been used as well.

One of the major goal of this work has been the physical parametrisation of the young stellar population in L1615/L1616. The spectral type classification has been performed by using a grid of reference spectra of giants, dwarfs, and intermediate templates, constructed by averaging spectra of giant and dwarf stars of the same spectral type. We have computed stellar luminosities by means of a SED fitting procedure properly developed by us, which also evaluates the interstellar/circumstellar reddening. This allowed us to derive the mass and age of each member of L1615/L1616 by comparing the location of the object on the H-R diagram with different sets of theoretical PMS evolutionary tracks.

Our analysis of the young population in L1615/L1616 yielded the following results:

- By using the  $H\alpha$  emission line intensity, as well as the strength of the lithium  $\lambda 6708 \text{ \AA}$  absorption line as main diagnostics of the PMS nature of the objects, we identified 25 new members of L1615/L1616, almost doubling the number of previously known young objects in this cloud.
- The age distribution of the L1615/L1616 population peaks between 1 and 3 Myr; however, the members of the cloud span a wide range in age, from  $\sim 0.1$  Myr up to 30 Myr, suggesting multiple events of star formation.
- The evidence of multiple star formation events, the spatial distribution of the classical and weak T Tauri populations, as well as the cloud shape, support the hypothesis of the star formation in L1615/L1616 being triggered by the massive stars in the nearby Orion OB associations.
- The slope of the IMF in L1615/L1616 in the mass range  $0.1 \leq M \leq 5.5 M_{\odot}$  is  $0.84 \pm 0.07$ , i.e. similar to that obtained in other star forming regions by different authors. This provides further support of a universal IMF in the stellar domain, regardless of the environmental conditions.

- The star formation efficiency is about 7–8 % as expected for molecular clouds in the vicinity of OB associations. According to the criterion by Lada & Lada (2003), L1615/L1616 is a small cluster with moderate star formation.
- A very low-fraction of possible sub-stellar objects ( $\sim 5\text{--}7\%$ ) is found in L1615/L1616; thus, the dynamical interaction with the close massive stars in the Orion OB associations and/or the photoevaporation induced by their ionising radiation do not appear as efficient triggering factors for BD formation.

We thank the anonymous referee for his/her careful reading, useful comments, and suggestions which helped to improve the manuscript. This paper is based on observations carried out at the European Southern Observatory, La Silla and Paranal (Chile), under observing programs numbers 64.I-0355, 70.C-0629, 70.C-0536, 074.C-0111 and 076.C-0385. The authors are grateful to Menadora Barcellona and Salvatore Spezzi for their supports during the preparation of this paper. We thank J. Hernandez for providing the calibration curves for spectral classification, and for discussions concerning the spectral classification of early-type stars. We are also grateful to Matula for her assiduous and warm assistance during the writing of this manuscript. This work was partially financed by the Istituto Nazionale di Astrofisica (INAF) through PRIN-INAF-2005. D.G. acknowledges financial support from PRIN-INAF-2005 (“Stellar clusters: a benchmark for star formation and stellar evolution”). This publication makes use of data products from the Two-Micron All-Sky Survey, which is a joint project of the University of Massachusetts and the Infrared Processing and Analysis Center/California Institute of Technology, funded by NASA and the National Science Foundation. This research has made use of the SIMBAD database, operated at CDS, Strasbourg, France. This paper includes data from the DENIS project, which has been partly funded by the SCIENCE and the HCM plans of the European Commission under grants CT920791 and CT940627.

## A. Spectral Type Classification

In order to find the template spectrum which better reproduces the target spectrum, we proceed as follows:

- We have first performed a spline interpolation of each standard spectra onto the wavelength points of the target spectrum. This allowed us to get a homogeneous wavelength



grid with the same step as the observed spectrum. Moreover, the spectral regions encompassing both the O<sub>3</sub> and H<sub>2</sub>O telluric bands near 6900, 7250, and 7600 Å, have been excluded in the fitting procedure.

- The standard spectra have been shifted in wavelength to the radial velocity of the target; a cross-correlation algorithm was used to find the velocity shift between the templates and target spectrum and superimpose each other.
- The extinction law derived by Cardelli et al. (1989) have been adopted to redden the wavelength-shifted standard spectra before comparing them to the observed one. We assumed a normal slope of the reddening law, i.e. we adopted a value of the ratio of total-to-selective extinction  $R_V = A_V/E(B - V)$  equal to 3.1. Each standard spectrum has been progressively reddened assuming an increasing value of the extinction in the V-band ( $A_V$ ); we let it vary from 0 to 15 mag, with a step of 0.05 mag.
- After each reddening step, the standard spectrum was subtracted to the observed one. The sum of the residuals was taken as indicator for the goodness of the “fit”. The reddened standard spectrum which gave the lowest value of this indicator provided the spectral type of the target as well as a first estimation of the extinction value  $A_V$ .

As an example, the FORS2 spectra of two PMS stars, namely RX J0507.6–0318 and RX J0507.4–0320, as well as the low- and the intermediate-resolution VIMOS spectra of TTS 050752.0–032003 are shown in Figure 9 and Figure 10, respectively; the best-fitting templates (thick lines) are superimposed on the observed spectra (thin lines). Note that the two VIMOS spectra yielded the same spectral type and a consistent value of  $A_V$ , well within the errors, regardless of the different resolving power and wavelength coverage.

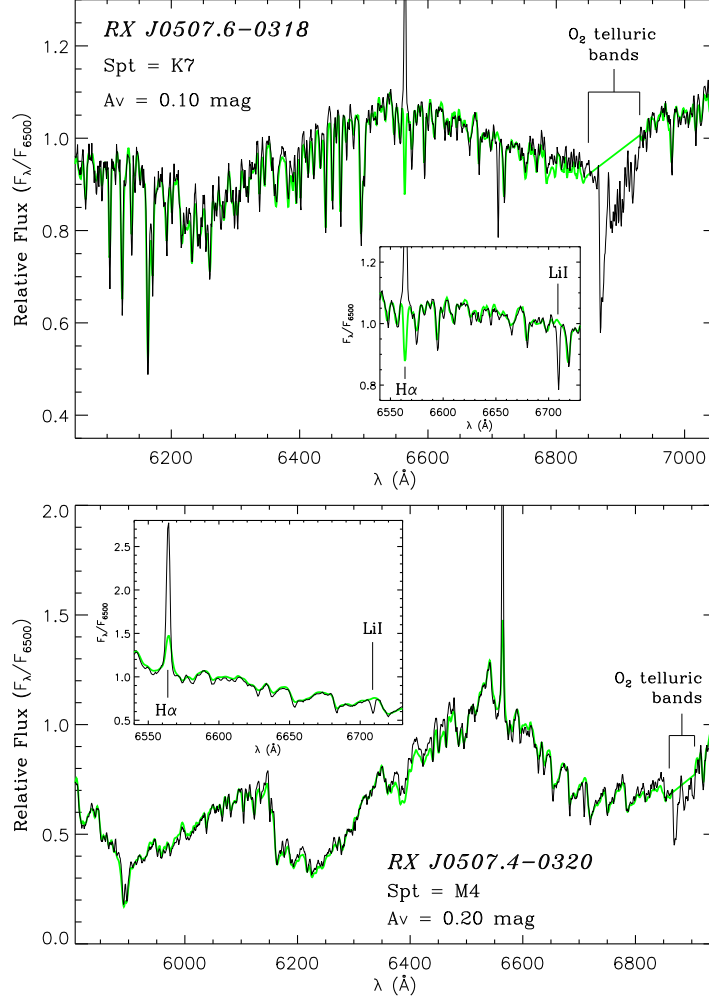


Fig. 9.— FORS2 spectra (thin lines) of RX J0507.6–0318 (upper panel) and RX J0507.4–0320 (lower panel). Overplotted with thick lines are the best-fitting K7 and M4 templates, reddened with  $A_V = 0.1$  and  $0.2$  mag, respectively, as derived by the spectrum fitting procedure. The spectra are arbitrarily normalised to the flux at  $6500$  Å. The  $O_2$  absorption telluric bands near  $\sim 6900$  Å are marked. This spectral region has been excluded in the fitting procedure. The LiI  $\lambda 6708$  Å absorption and the  $H\alpha$  emission lines are shown in more detail in the inset of each panel. Note the differences in  $H\alpha$  and LiI between the template and the observed spectra, confirming the PMS nature of the two stars. Also note the good agreement in the two independent determinations of  $A_V$ , as obtained from the spectral type classification and the SED fitting procedure (Table 5).

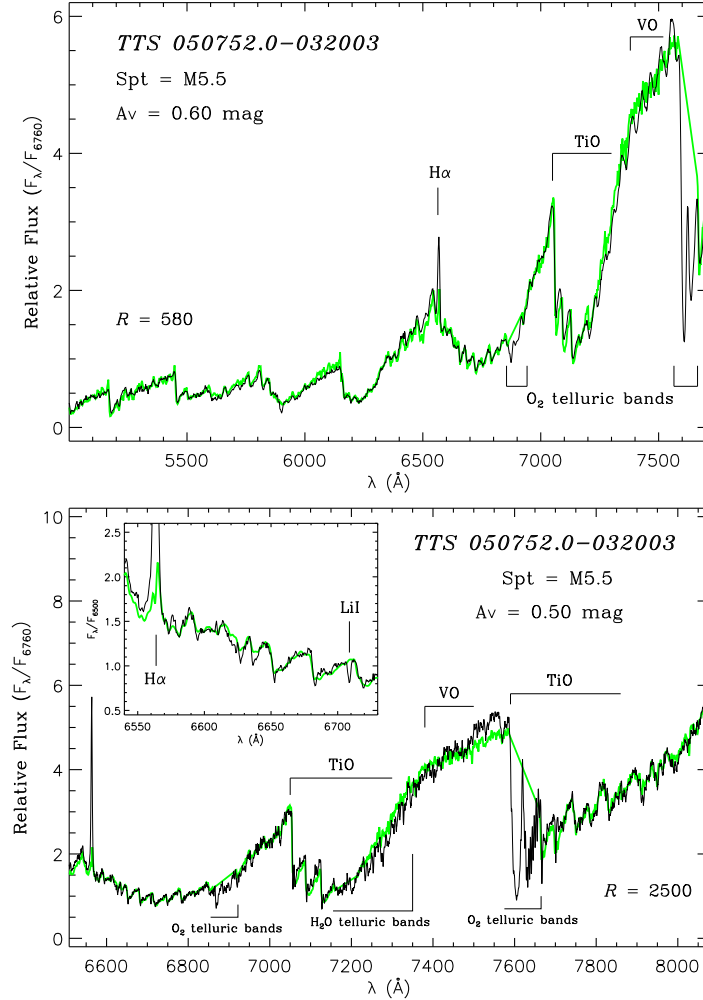


Fig. 10.— Low- (upper panel) and intermediate-resolution (lower panel) VIMOS spectra of TTS 050752.0–032003. The observed spectra are displayed with thin lines, while the best-fitting M5.5 template, reddened with  $A_V = 0.6$  and  $0.5$  mag, respectively, is overplotted with a thick line. The spectra have been arbitrarily normalised to the flux at  $6760$  Å. The O<sub>2</sub> absorption telluric bands near  $\sim 6900$  and  $\sim 7600$  Å, as well as the H<sub>2</sub>O one near  $\sim 7250$  Å are marked. Note that these spectral regions have been excluded in the fitting procedure. The main TiO and VO bands are marked also. The Li I  $\lambda 6708$  Å absorption and the  $H\alpha$  emission lines are shown in more detail in the inset of the lower panel. Note the differences in  $H\alpha$  and Li I between the template and the observed spectra, confirming the PMS nature of the star. Also note the good agreement between the two values of  $A_V$  and the one derived from the SED fitting procedure (Table 5).

## B. SED fitting procedure

The method we employed to determine both the reddening parameters (i.e.  $A_V$  and  $R_V$ ) and the stellar intrinsic properties (i.e.  $R_\star$  and  $L_\star$ ) of each PMS star, is based on the use of appropriate stellar atmosphere models. Taking into account the effective temperature range of the L1615/L1616 members (see Table 5), as well as the wide wavelength coverage required to encompass their SEDs (see Table 6), we merged three distinct sets of low-resolution synthetic spectra, adopting the following criteria:

- for the two intermediate-mass stars, namely the B9V-type HD 293815 and the Herbig B3e-type star Kiso A-0974 15, we chose the grid of stellar atmosphere models computed by Kurucz (1979);
- for sources covering the effective temperature interval between 4000 and 10000 K we used the low-resolution synthetic spectra calculated by Hauschildt et al. (1999) with their *NextGen* model-atmosphere code;
- for objects cooler than 4000 K we used the synthetic low-resolution *StarDusty* spectra for low-mass stars and BDs by Allard et al. (2000). The *StarDusty* spectra, which take into account dust grain formation in the model atmosphere due to an efficient gravitational settling process, are the most suitable for simulating cool objects, down to the very low-mass end. Indeed, Allard et al. (2001) found that silicate dust grains can form abundantly in the outer atmospheric layers of the latest M dwarfs and BDs.

Each set of atmosphere models contains flux density spectra at the stellar surface, computed for different value of gravity and metallicity. We kept the gravity of the atmosphere models to a fixed value of  $\log(g) = 4.0$  (cgs units), which is appropriate for low-mass stars and BDs younger than 10 Myr (Chabrier et al. 2000). Furthermore, this value closely matches the one expected for H AeBe and early type main sequence stars (Kurucz 1979; Schmidt-Kaler 1982). We also adopted a solar metallicity. However, we remind the reader that Romaniello et al. (2002) have analysed the influence of gravity and metallicity on the fitting-procedure and found that neither of them affects the values of the derived parameters significantly.

A grid of models matching the adopted effective temperature scale (see Section 5.2) was first derived by performing a linear interpolation of the merged set of synthetic spectra. In order to compare the observed SEDs with theoretical ones, synthetic magnitudes in the same photometric systems in which the observations were performed are required. Thus, for each adopted temperature we derived a look-up table of synthetic  $UBVR_CI_CJHKs$

absolute magnitudes by reddening the corresponding theoretical spectrum with an increasing value of  $A_V$  (from 0 to 15 mag with a step of 0.05 mag) and  $R_V$  (from 1 to 9 with a step of 0.1), and subsequently integrating the reddened spectrum over each photometric pass-band. The extinction law by Cardelli et al. (1989) was adopted to perform this reddening procedure. Since the model spectra are given as flux density at the star’s surface, the synthetic magnitudes were computed for a star<sup>7</sup> with one solar radius, as seen from a distance of 10 pc. The Johnson-Cousins  $UBVR_CI_C$  and 2MASS  $JHK_s$  transmission curves from *The Asiago Database on Photometric Systems* (Moro & Munari 2000; Fiorucci & Munari 2002), as well as the absolute flux calibration constants reported in Table 6 were used to integrate each progressively reddened theoretical spectra.

Finally, the values of  $A_V$  and  $R_V$  of each PMS star (see Table 5) were derived simultaneously by fitting the corresponding observed SED to the look-up table of reddened synthetic magnitudes having the same effective temperature as the given object. In order to eliminate the magnitude shift introduced by the unknown star’s radius and distance, the observed and the synthetic magnitudes were previously normalised to the  $I_C$ -band. For PMS stars showing clear evidence of near-infrared excess associated with the presence of circumstellar material, the fit was performed to the short-wavelength portion ( $\lambda \leq \lambda_J$ ) of the SED, which is less contaminated by near-infrared excess. The error on  $A_V$  and  $R_V$  has been evaluated taking into account both the accuracy on the spectral type classification (Section 5.2) and the photometric errors on the observed magnitudes.

An example of the output of the fitting procedure is shown in the upper panel of Figure 11, where a contour plot of the  $\chi^2$  value in the  $R_V$ - $A_V$  plane is reported. As already stated in Section 5.3, our two-parameter fitting procedure can be applied only to stars which suffer a visual extinction larger than about 0.5 mag. For low-reddened stars the value of  $A_V$  is fairly independent of changes in  $R_V$ . As clearly evident in the lower panel of Figure 11, in this case a unique solution could not be found simultaneously in the  $R_V$ - $A_V$  plane. Therefore, the value of  $R_V = 3.1$ , typical of the diffuse interstellar medium, was assumed for all the object with  $A_V \lesssim 0.5$  mag.

Once the extinction parameters were determined, the value of  $R_\star$  for each PMS object was obtained from the magnitude shifts required to match the observed magnitudes to the theoretical ones, reddened with the best-fitting  $A_V$  and  $R_V$ . Only the photometric bands actually used in the fitting procedure for each given object were employed to determine its stellar radius. As suggested by Alcalá et al. (2004), we made the assumption that all

---

<sup>7</sup>This choice is only conventional, since at this step we were only interested in the shape of the flux distribution.

the members of L1615/L1616 are located at  $450 \pm 20$  pc. Finally the value of  $L_\star$  was derived assuming a black body emission at the star’s effective temperature and radius. The associated uncertainties were derived taking into account the errors on the distance and effective temperature.

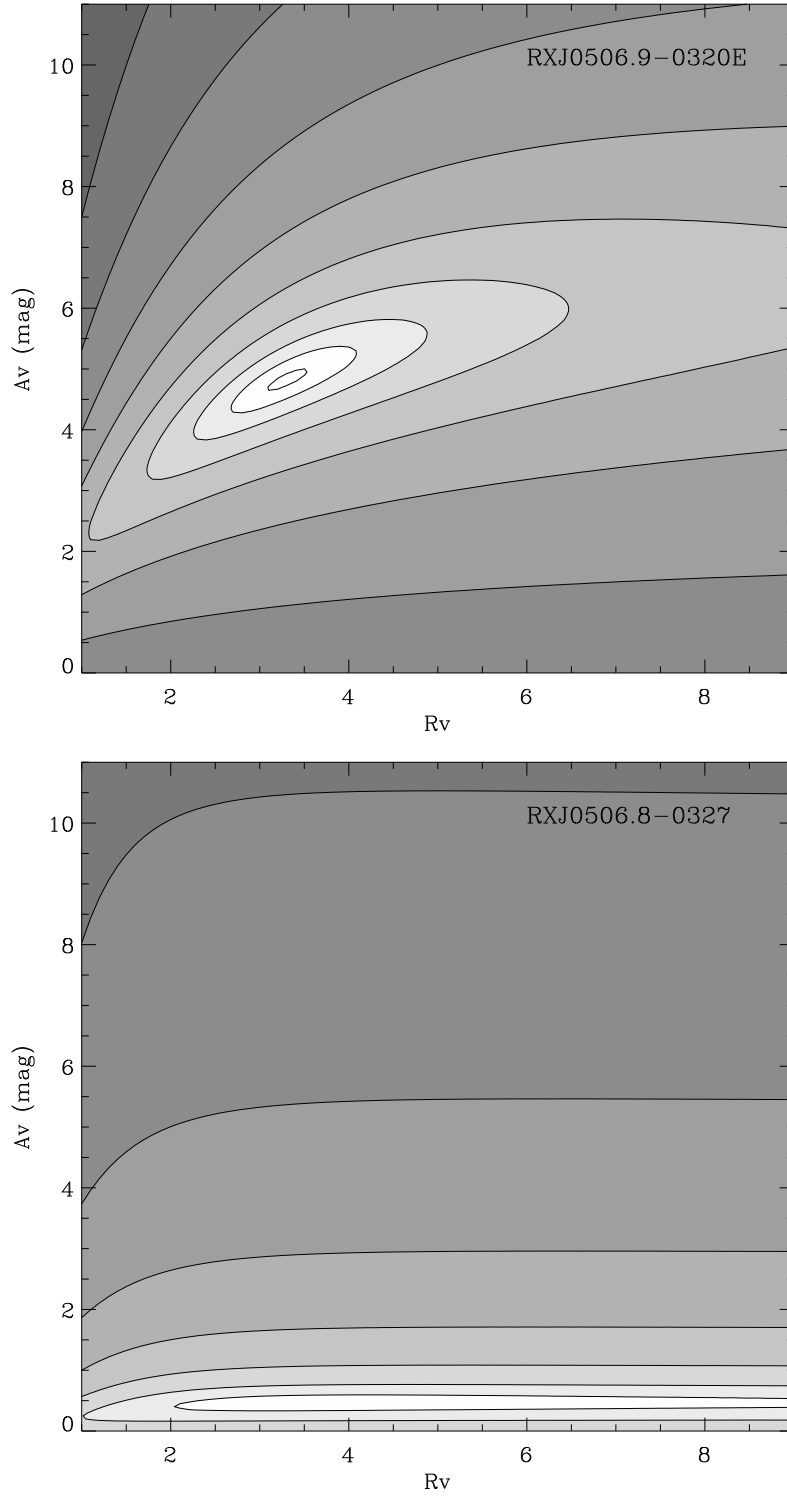


Fig. 11.—  $\chi^2$  contour plots produced by the SED fitting procedure for the two stars RX J0506.9–0320E and RX J0506.8–0327.

## REFERENCES

- Alcalá J.M., Krautter J., Schmitt J.H.M.M. et al. 1995, A&AS 114, 109
- Alcalá J.M., Terranegra, L., Wichmann, R. et al. 1996, A&A 119, 7
- Alcalá J.M., Wachter S., Covino E. et al. 2004, A&A 416, 677
- Alcalá J.M., Spezzi L., Frasca A. et al. 2006, A&A 453, L1
- Alcalá J.M., Spezzi L., Chapman, N. et al. 2006, ApJ 676, 427
- Allard F., Hauschildt P.H. & Schwenke D. 2000, ApJ 540, 1005
- Allard F., Hauschildt P.H., Alexander D.R. et al. 2001, ApJ 556, 357
- Appenzeller I., Fricke K., Furtig, W. et al. 1998, *The Messenger* 94, 1
- Baraffe I., Chabrier G., Allard F. et al. 1998, A&A 337, 403
- Baraffe I., Chabrier G., Allard F. & Hauschildt P.H. 2002, A&A 382, 563
- Barrado Y Navascuès D., Stauffer J.R., Bouvier J. & Martínet E.L. 1998, Ap&SS 263, 1-4,303
- Barrado Y Navascuès D., Bouvier J., Stauffer J.R. et al. 2002, A&A 395, 813
- Barrado Y Navascuès D., Stauffer J.R., Bouvier J. et al. 2004, ApJ 610, 1064
- Basri G. & Batalha C. 1990, ApJ 363, 654
- Bèjar V.J.S., Martín E.L., Zapatero Osorio M. R. et al. 2001, ApJ 556, 830
- Bertin E. & Arnouts S. 1996, A&AS 117, 393
- Blecha A., Cayatte V., North P. et al. 2000, SPIE 4008, 467
- Bochanski J.J., West A.A., Hawley S.L. et al. 2007, AJ 133, 531
- Bodenheimer P. 1965, ApJ 142, 451
- Bohlin R.C., Savage B.D. & Drake J.F. 1978, ApJ 224, 132
- Briceño C., Luhman K.L., Hartmann L. et al. 2002, ApJ 580, 317
- Cardelli J.A., Clayton G.C. & Mathis J.S. 1989, ApJ 345, 245
- Carpenter J.M. 2001, AJ 121, 2851



- Chabrier G., Baraffe I., Allard F. & Hauschildt P.H. 2000, ApJ 542, 464
- Cieslinski D., Jablonski F.J. & Steiner J.E. 1997, A&AS 124, 55
- Clark P.C., Bonnell I.A., Zinnecker H. & Bate M.R. 2005, MNRAS 359, 809
- Cohen M. & Kuhl L.V. 1979, ApJS 41, 743
- Cohen M., Wheaton W.A. & Megeath S.T. 2003, AJ 126, 1096
- Covino E., Alcalá J.M., Allain S. et al. 1997, A&A 328, 187
- Comeron F., Neuhäuser R. & Kaas A.A. 2000, A&A 359, 269
- Cousins A.W.J. 1976, MmRAS 81, 25
- Cutri R.M., Skrutskie M.F., van Dyk S. et al. 2003, *2MASS All-Sky Catalog of Point Sources*, NASA/IPAC Infrared Science Archive
- D’Antona F. & Mazzitelli I. 1997, Mem. S.A.It. 68, 807
- Droege T.F., Richmond M.W., Sallman M.P., Creager R.P. 2006, PASP 118, 1666
- Epchtein, N., et al. 1997, Messenger, 87, 27
- Feigelson E.D. & Montmerle T. 1999, ARA&A 37, 363
- Fiorucci M. & Munari U. 2002, Ap&SS 280, 77
- Frasca A., Alcalá J.M., Covino E. et al. 2003, A&A 405, 149
- Frasca A., Guillout P., Marilli E. et al. 2006, A&A 454, 301
- Guillout P., Sterzik M.F., Schmitt J.H.M.M. et al. 1998, A&A 334, 540
- Guillout P., Sterzik M.F., Schmitt J.H.M.M. et al. 1998, A&A 337, 113
- Guieu S., Dougados C., Monin J.-L. et al. 2006, A&A 446, 485
- Hamuy M., Walker A.R., Suntzeff N.B. et al. 1992, PASP 104, 533
- Hamuy M., Suntzeff N.B., Heathcote S.R. et al. 1994, PASP 106, 566
- Harvey, P., et al. 2007, ApJ, 663, 1139 (H07)
- Hauschildt P.H., Allard F. & Baron E. 1999, ApJ 512, 377

- Hawley S.L., Covey K.R., Knapp G.R. et al. 2002, AJ 123, 3409
- Helou G. & Walker D.W. 1988, Infrared Astronomical Satellite (IRAS) Catalogs and Atlases, Vol.7: *The Small Scale Structure Catalog* (NASA RP-1190; Washington: GPO)
- Herbst W., Warner J.W., Miller D.P. et al. 1982, AJ 87, 98
- Hernández J., Calvet N., Briceño C. et al. 2004, AJ 127, 1682
- Hillenbrand L.A. & Carpenter J. 2000, ApJ 540, 236
- Izzo C., Kornweibel N., McKay D. et al. 2004, Msngr 177, 33
- Johnson H.L. 1965, ApJ 141, 923
- Jørgensen, J.K., et al., 2007, ApJ, submitted
- Kainulainen J., Lehtinen K. & Harju J. 2006, A&A 447, 597
- Kenyon S.J. & Hartmann L. 1995, ApJS 101, 117
- Kroupa P. 2001, MNRAS 322, 231
- Kroupa P. 2002, Science Vol. 295, Issue 5552, pag. 82
- Kun M., Prusti T., Nikolic S., Johansson L.E.B. & Walton N.A. 2004, A&A 418, 89
- Kurucz R.L. 1979, ApJS 40, 191
- Lada, C.J., Lada, E.A., A.R.A&A, 41, 57 (LL03)
- Lada, C.J., Muench, A.A., Luhman, K.L., et al. 2006, AJ 131, 1574
- Landolt A.U. 1992, AJ 104, 340
- Lee T.A. 1968, ApJ 152, 913
- Lee H.-T., Chen W.P., Zhang Z.-W. & Hu J.-Y. 2005, ApJ 624, 808
- Lee H.-T. & Chen W.P. 2007, ApJ 657, 884
- Le Borgne J.F., Bruzual G., Pelló R. et al. 2003, A&A 402, 433
- LeFevre O., Saisse M., Mancini D. et al. 2003, SPIE 4841, 1670
- Leggett S.K., Allard F., Berriman G. et al. 1996, ApJS 104, 117

- Lombardi, M., & Alves, J. 2001, A&A, 377, 1023
- López Martí B., Eislöffel J., Scholz A. & Mundt R. 2004, A&A 416, 555
- Luhman K.L. 1999, ApJ 525, 466
- Luhman K.L. & Rieke G.H. 1999, ApJ 525, 440
- Luhman K.L., Rieke G.H., Young E.T. et al. 2000, ApJ 540, 1016
- Luhman K.L., Stauffer J.R., Muench A.A. et al. 2003, ApJ 593, 1093
- Lynds B.T. 1962, ApJS 7, 1L
- Lynds B.T. 1965, ApJS 12, 163
- Maddalena R.J., Morris M., Moscowitz J. & Thaddeus P. 1986, ApJ 303, 375
- Marilli E., Frasca A., Covino E. et al. 2007, A&A 463, 1081
- Martín E.L., Delfosse X., Basri G. et al. 1999, AJ 118, 2466
- Merín et al., 2007, ApJ, submitted
- Mermilliod J.C., Mermilliod M., & Hauck B. 1997, A&AS, 124, 349
- Miller G.E. & Scalo J.M. 1979, ApJS 41, 513
- Morau E., Bouvier J., Stauffer J.R. et al. 2003, A&A 400, 891
- Moro D. & Munari U. 2000, A&AS 147, 361
- Muench A.A., Lada E.A., Lada C.J. et al. 2002, ApJ 573, 366
- Muench A.A., Lada E.A., Lada C.J. et al. 2003, AJ 125, 2029
- Mundt R. & Bastian U. 1980, A&AS 39, 245
- Nakano M., Wiramihardja S.D. & Kogure T. 1995, PASJ 47, 889
- Oke J.B. 1990, AJ 99, 1621
- Palla F. & Stahler S.W. 1999, ApJ 525, 772
- Pasquini L., Avila G., Blecha A. et al. 2002, *The Messenger* 110, 1

- Persson, S. E., Murphy, D. C., Krzeminski, W., Roth, M., & Rieke, M. J. 1998, AJ, 116, 2475
- Preibisch T., Stanke T. & Zinnecker H. 2003, A&A 409, 147
- Ramesh B. 1995, MNRAS 276, 923
- Romaniello R., Panagia N., Scuderi S. et al. 2002, AJ 123, 915
- Romaniello R., Scuderi S., Panagia N. et al. 2006, A&A 446, 955
- Schmidt-Kaler Th. 1982, in Landoldt-Börnstein, New Ser., ed. K.H. Hellwege, Vol. VI/2b (Springer-Verlag, Berlin, Heidelberg, New York), 12
- Scodeggio M., Franzetti P., Garilli B. et al. 2005, PASP 117, 1284
- Sharpless S. 1952, ApJ 116, 251
- Spezzi L., Alcalá J.M., Fasca A., Covino E. & Gandolfi D. 2007, A&A, 470, 281
- Spezzi L., Alcalá J.M., Covino E., et al. 2008, ApJ, in press (arXiv:0802.4351)
- Stanke T., Smith M.D., Gredel R. et al. 2002, A&A 393, 251
- Sterzik M.F., Alcalá J.M., Neuhäuser R. et al. 1995, A&A 297, 418
- Stetson P.B. 1987, PASP 99, 191
- Taylor B.J., Joner M.D. & Johnson S.B. 1989, AJ 97, 1798
- Tej A., Sahu K.C., Chandrasekhar T. & Ashok N.M. 2002, ApJ 578, 523
- Thé P.S., Tjin-A-Djie H.R.E., Bakker R. et al. 1981, A&AS 44, 451
- Torres-Dodgen A.V. & Weaver W.B. 1993, PASP 105, 693
- Valdes F., Gupta R., Rose J.A. et al. 2004, ApJS 152, 251
- van Belle G.T., Lane B.F., Thompson R.R. et al. 1999, AJ 117, 521
- Vieira S.L.A., Corradi W.J.B., Alencar S.H.P. et al. 2003, AJ 126, 2971
- Voges W., Aschenbach B., Boller Th. et al. 1999, A&A 349, 389
- Warmels R.H. 1992, in *Astronomical Data Analysis Software and Systems I*, D.M. Worrall, C. Biemesderfer & J. Barnes eds., ASP Conf. Series Vol. 25, 115

- Waters, L.B.F.M. & Waelkens C. 1998, ARA&A 36, 233
- White, R. J. & Basri, G. 2003, ApJ 582, 1109
- Whittet D.C.B., Gerakines P.A., Hough J.H. et al. 2001, ApJ 547, 872
- Yonekura Y., Hayakawa T., Mizuno N et al. 1999, PASJ 51, 837
- Zickgraf F.J., Krautter J., Reffert S. et al. 2005, A&A 433, 151

Table 1. Journal of the FORS2 and VIMOS spectroscopic observations.

Spectrograph	Period	Grism	Order sorting filter	$\lambda/\Delta\lambda^*$	$\lambda_{range}$ (Å)	$T_{exp}$ (sec)	$N_{mask}$	$N_{object}$ per mask
FORS2@VLT	Feb–Mar 2003	GRIS-1200R	GG435	2140	5700–7300 <sup>†</sup>	960	5	18–19
VIMOS@VLT	Dec 2004–Mar 2005	HR_red	GG475	2500	6300–8700 <sup>†</sup>	2000	3	~ 80
VIMOS@VLT	Dec 2004–Mar 2005	MR	GG475	580	5000–8000	900	6	~ 120

\*Achieved at  $\lambda = 6500$  Å with a 1'' slit width.

<sup>†</sup>Corresponding to a slit projected onto the centre of the detector.

Table 2. PMS stars in L1615/L1616. Coordinates are from the 2MASS catalogue. The PMS objects identified in this work and the previously known ones are labelled with “NEW” and “P.K.”, respectively. For each star, additional designations found in literature are listed in the last column.

Star	$\alpha(2000)$ (hh:mm:ss)	$\delta(2000)$ (dd:mm:ss)	Note	Other Designations
1RXS J045912.4–033711	04:59:14.59	–03:37:06.3	P.K.	
1RXS J050416.9–021426	05:04:15.93	–02:14:50.5	P.K.	
TTS 050513.5–034248	05:05:13.47	–03:42:47.8	NEW	
TTS 050538.9–032626	05:05:38.85	–03:26:26.4	NEW	
RX J0506.6–0337	05:06:34.95	–03:37:15.9	P.K.	
TTS 050644.4–032913	05:06:44.42	–03:29:12.8	NEW	
TTS 050646.1–031922	05:06:46.05	–03:19:22.4	P.K.	
RX J0506.8–0318	05:06:46.64	–03:18:05.6	P.K.	
TTS 050647.5–031910	05:06:47.45	–03:19:09.7	NEW	
RX J0506.8–0327	05:06:48.32	–03:27:38.2	P.K.	
RX J0506.8–0305 <sup>a</sup>	05:06:48.98	–03:05:42.9	NEW	
TTS 050649.8–031933	05:06:49.77	–03:19:33.1	NEW	
TTS 050649.8–032104	05:06:49.78	–03:21:03.6	NEW	1RXS J050651.9–032031
TTS 050650.5–032014	05:06:50.50	–03:20:14.3	NEW	
TTS 050650.7–032008	05:06:50.74	–03:20:08.0	NEW	
RX J0506.9–0319NW	05:06:50.83	–03:19:35.2	P.K.	
RX J0506.9–0319SE	05:06:50.99	–03:19:38.0	P.K.	L1616 MIR5
HD 293815	05:06:51.05	–03:19:59.9	P.K.	
RX J0506.9–0320W	05:06:52.86	–03:20:53.2	P.K.	L1616 MIR2
RX J0506.9–0320E	05:06:53.32	–03:20:52.6	P.K.	L1616 MIR1
TTS 050654.5–032046	05:06:54.53	–03:20:46.0	NEW	
LkH $\alpha$ 333	05:06:54.65	–03:20:04.8	P.K.	HBC 82, Kiso A-0974 14, CSI-03-05045
L1616 MIR4 <sup>b</sup>	05:06:54.93	–03:21:12.7	P.K.	
Kiso A-0974 15	05:06:55.52	–03:21:13.2	P.K.	NSV 1832, IRAS 05044–0325, L1616 MIR3
RX J0507.0–0318	05:06:56.94	–03:18:35.5	P.K.	
TTS 050657.0–031640	05:06:56.97	–03:16:40.4	NEW	
TTS 050704.7–030241	05:07:04.71	–03:02:41.0	NEW	
TTS 050705.3–030006	05:07:05.32	–03:00:06.2	NEW	
RX J0507.1–0321	05:07:06.10	–03:21:28.2	P.K.	Kiso A-0974 16
TTS 050706.2–031703	05:07:06.22	–03:17:02.9	NEW	
RX J0507.2–0323	05:07:10.95	–03:23:53.4	P.K.	Kiso A-0974 18
TTS 050713.5–031722	05:07:13.52	–03:17:22.1	NEW	
RX J0507.3–0326 <sup>a</sup>	05:07:14.99	–03:26:47.3	NEW	
TTS 050717.9–032433	05:07:17.85	–03:24:33.1	P.K.	
RX J0507.4–0320	05:07:22.28	–03:20:18.5	P.K.	
RX J0507.4–0317 <sup>a</sup>	05:07:25.93	–03:17:12.3	NEW	

Table 2—Continued

Star	$\alpha(2000)$ (hh:mm:ss)	$\delta(2000)$ (dd:mm:ss)	Note	Other Designations
TTS 050729.8–031705	05:07:29.80	–03:17:05.1	NEW	
TTS 050730.9–031846	05:07:30.85	–03:18:45.6	NEW	
TTS 050733.6–032517	05:07:33.58	–03:25:16.7	NEW	
TTS 050734.8–031521	05:07:34.83	–03:15:20.7	NEW	
RX J0507.6–0318 <sup>a</sup>	05:07:37.67	–03:18:15.6	NEW	
TTS 050741.0–032253	05:07:41.00	–03:22:53.0	NEW	
TTS 050741.4–031507	05:07:41.35	–03:15:06.7	NEW	
TTS 050752.0–032003	05:07:51.95	–03:20:02.8	NEW	
TTS 050801.4–032255	05:08:01.43	–03:22:54.5	P.K.	
TTS 050801.9–031732	05:08:01.94	–03:17:31.6	P.K.	
TTS 050804.0–034052	05:08:04.00	–03:40:51.7	P.K.	
TTS 050836.6–030341	05:08:36.55	–03:03:41.4	P.K.	Kiso A-0974 21
TTS 050845.1–031653	05:08:45.10	–03:16:52.5	P.K.	
RX J0509.0–0315	05:09:00.66	–03:15:06.6	P.K.	1RXS J050859.6–031503
RX J0510.1–0427	05:10:04.60	–04:28:03.7	P.K.	1RXS J051004.9–042757
1RXS J051011.5–025355	05:10:10.86	–02:54:04.9	P.K.	V1011 Ori, IRAS 05076–0257
RX J0510.3–0330	05:10:14.78	–03:30:07.4	P.K.	1RXS J051015.7–033001
1RXS J051043.2–031627	05:10:40.50	–03:16:41.6	P.K.	RXJ 0510.7–0316
RX J0511.7–0348	05:11:38.93	–03:48:47.1	P.K.	
RX J0512.3–0255	05:12:20.53	–02:55:52.3	P.K.	V531 Ori, 1RXS J051219.9–025547

<sup>a</sup>X-ray source by Alcalá et al. (2004)

<sup>b</sup>Mid-infrared source by Stanke et al. (2002)



Table 3. Optical ( $UBVR_CI_C$ ) and near-infrared ( $JHKs$ ) photometry of the PMS stars in L1615/L1616. Labels are as explained in the footnotes.

PMS Star	$U$	$B$	$V$	$R_C$	$I_C$	$J$	$H$	$Ks$	Notes
1RXS J045912.4–033711	12.74±0.05	12.45±0.04	11.73±0.03	NO	10.72±0.06	10.07±0.02	9.62±0.02	9.47±0.02	a,b,c
1RXS J050416.9–021426	14.84±0.09	13.99±0.08	12.96±0.02	NO	11.59±0.03	10.66±0.02	10.10±0.02	9.98±0.03	a,c,d
TTS 050513.5–034248	NO	ND	ND	18.97±0.02	17.03±0.02	15.12±0.04	14.60±0.05	14.20±0.06	c
TTS 050538.9–032626	NO	18.88±0.02	17.30±0.02	16.21±0.02	14.67±0.01	13.29±0.02	12.60±0.02	12.39±0.02	c
RX J0506.6–0337	13.12±0.04	12.93±0.02	12.23±0.01	NO	11.24±0.05	10.66±0.02	10.30±0.03	10.20±0.02	a,b,c
TTS 050644.4–032913	NO	19.33±0.01	17.69±0.02	16.68±0.02	15.08±0.01	13.64±0.03	13.04±0.03	12.78±0.03	c
TTS 050646.1–031922	NO	18.88±0.01	17.34±0.02	16.09±0.01	14.81±0.01	12.60±0.01	11.09±0.01	10.22±0.01	
RX J0506.8–0318	NO	16.26±0.01	14.86±0.02	13.91±0.01	13.01±0.01	11.95±0.01	11.22±0.01	10.97±0.01	
TTS 050647.5–031910	NO	22.55±0.12	20.51±0.03	19.01±0.03	16.75±0.02	14.30±0.01	13.38±0.01	13.04±0.01	
RX J0506.8–0327	NO	17.59±0.01	15.96±0.02	14.90±0.02	13.30±0.01	11.74±0.01	10.92±0.01	10.59±0.01	
RX J0506.8–0305	NO	18.99±0.01	17.33±0.02	16.23±0.02	14.59±0.01	13.02±0.01	12.39±0.01	12.13±0.01	
TTS 050649.8–031933	NO	19.42±0.03	17.63±0.02	16.32±0.02	14.48±0.01	12.44±0.01	11.52±0.01	11.18±0.01	
TTS 050649.8–032104	NO	19.91±0.02	18.59±0.02	17.30±0.02	15.56±0.01	12.69±0.01	11.43±0.01	10.51±0.01	
TTS 050650.5–032014	NO	23.58±0.77	21.11±0.05	19.18±0.03	16.51±0.02	13.78±0.01	13.09±0.01	12.60±0.01	
TTS 050650.7–032008	NO	21.50±0.13	19.54±0.03	18.14±0.02	16.03±0.02	13.78±0.01	13.07±0.01	12.59±0.01	
RX J0506.9–0319NW	NO	18.18±0.01	16.73±0.02	15.70±0.02	14.31±0.01	12.46±0.01	11.60±0.01	11.33±0.01	
RX J0506.9–0319SE	NO	16.34±0.01	14.82±0.02	13.80±0.02	12.67±0.01	11.09±0.01	10.16±0.01	9.97±0.01	
HD 293815	10.33±0.01	10.28±0.01	10.08±0.01	9.94±0.01	9.77±0.01	9.50±0.02	9.48±0.03	9.37±0.03	c,e
RX J0506.9–0320W	NO	17.36±0.01	15.33±0.02	13.94±0.02	12.39±0.01	10.66±0.01	9.51±0.01	8.94±0.01	
RX J0506.9–0320E	NO	17.66±0.01	15.74±0.02	14.36±0.02	12.87±0.01	10.75±0.01	9.51±0.01	8.76±0.01	
TTS 050654.5–032046	NO	ND	ND	20.98±0.08	18.92±0.03	15.92±0.02	14.92±0.01	14.23±0.01	
LkH $\alpha$ 333	16.55±0.02	15.74±0.01	14.19±0.01	S	S	10.34±0.02	9.24±0.02	8.44±0.03	c,f
L1616 MIR4	NO	21.12±0.13	18.99±0.04	17.59±0.02	15.94±0.01	12.78±0.02	10.83±0.01	9.66±0.01	
Kiso A-0974 15	13.54±0.01	13.65±0.01	12.84±0.01	12.18±0.01	11.42±0.01	9.89±0.03	9.13±0.03	8.49±0.03	c,g
RX J0507.0–0318	NO	16.89±0.01	15.21±0.02	14.08±0.02	12.91±0.01	11.48±0.01	10.48±0.01	10.13±0.01	
TTS 050657.0–031640	NO	18.80±0.01	17.69±0.02	16.48±0.02	14.88±0.01	13.12±0.01	12.48±0.01	12.11±0.01	
TTS 050704.7–030241	NO	21.87±0.04	20.04±0.02	18.81±0.02	16.75±0.02	14.94±0.01	14.32±0.01	14.00±0.01	
TTS 050705.3–030006	NO	16.95±0.01	15.50±0.02	14.55±0.02	13.60±0.01	12.63±0.01	11.75±0.01	11.63±0.01	
RX J0507.1–0321	NO	17.56±0.01	16.13±0.02	15.08±0.02	13.87±0.01	12.40±0.01	11.53±0.01	11.20±0.01	
TTS 050706.2–031703	NO	21.83±0.04	19.99±0.02	18.71±0.02	16.66±0.02	14.69±0.01	14.18±0.01	13.84±0.01	
RX J0507.2–0323	NO	15.09±0.01	13.95±0.01	S	12.61±0.02	11.79±0.01	11.01±0.01	10.95±0.01	d
TTS 050713.5–031722	NO	19.09±0.01	17.57±0.02	16.55±0.01	15.61±0.01	14.05±0.01	13.02±0.01	12.61±0.01	
RX J0507.3–0326	NO	15.72±0.01	14.31±0.01	13.42±0.02	12.58±0.02	11.45±0.02	10.78±0.02	10.63±0.02	c,d
TTS 050717.9–032433	NO	18.24±0.01	16.67±0.02	15.64±0.01	14.40±0.01	13.17±0.01	12.48±0.01	12.23±0.01	
RX J0507.4–0320	NO	18.37±0.01	16.71±0.02	15.58±0.01	13.98±0.01	12.42±0.01	11.73±0.01	11.49±0.01	h

Table 3—Continued

PMS Star	$U$	$B$	$V$	$R_C$	$I_C$	$J$	$H$	$Ks$	Notes
RX J0507.4–0317	NO	18.68±0.01	17.19±0.02	16.17±0.02	14.70±0.01	13.25±0.01	12.61±0.01	12.34±0.01	
TTS 050729.8–031705	NO	22.77±0.08	20.83±0.03	19.39±0.02	17.16±0.02	14.94±0.04	14.23±0.04	13.96±0.05	c
TTS 050730.9–031846	NO	ND	22.12±0.08	21.09±0.04	18.93±0.02	16.49±0.03	15.94±0.03	15.40±0.02	
TTS 050733.6–032517	NO	21.36±0.03	19.62±0.02	18.39±0.02	16.49±0.02	14.79±0.01	14.21±0.01	13.90±0.01	
TTS 050734.8–031521	NO	20.59±0.02	19.05±0.02	17.85±0.02	16.10±0.01	14.51±0.01	13.87±0.01	13.60±0.01	
RX J0507.6–0318	NO	16.52±0.01	15.16±0.02	14.27±0.01	13.42±0.01	12.44±0.01	11.71±0.01	11.50±0.01	
TTS 050741.0–032253	NO	19.16±0.01	17.55±0.02	16.51±0.02	14.96±0.01	13.52±0.03	12.81±0.03	12.57±0.03	c
TTS 050741.4–031507	NO	19.43±0.01	17.92±0.02	16.86±0.02	15.13±0.01	13.60±0.01	12.90±0.01	12.66±0.01	
TTS 050752.0–032003	NO	21.30±0.03	19.55±0.02	18.27±0.02	16.32±0.02	14.52±0.03	13.98±0.04	13.51±0.04	c
TTS 050801.4–032255	NO	NO	NO	NO	13.82±0.04	12.51±0.02	11.63±0.02	11.23±0.02	c,d
TTS 050801.9–031732	NO	NO	NO	NO	13.84±0.04	12.39±0.02	11.66±0.02	11.33±0.03	c,d
TTS 050804.0–034052	NO	NO	NO	NO	14.28±0.04	13.00±0.03	12.33±0.03	12.07±0.02	c,d
TTS 050836.6–030341	NO	NO	NO	NO	13.46±0.03	11.93±0.02	11.16±0.03	10.73±0.02	c,d
TTS 050845.1–031653	NO	NO	NO	NO	13.88±0.04	12.37±0.04	11.82±0.04	11.46±0.03	c,d
RX J0509.0–0315	12.26±0.04	12.09±0.03	11.39±0.02	NO	10.51±0.04	9.91±0.02	9.53±0.02	9.41±0.02	a,b,c
RX J0510.1–0427	13.36±0.01	12.65±0.01	11.73±0.01	NO	10.41±0.05	9.68±0.02	9.14±0.03	8.99±0.02	a,b,c
1RXS J051011.5–025355	14.27±0.24	13.43±0.23	12.42±0.23	11.81±0.23	11.24±0.23	10.45±0.02	9.95±0.02	9.73±0.02	c,i
RX J0510.3–0330	NO	12.53±0.04	11.74±0.03	11.29±0.02	10.87±0.02	10.04±0.15	9.81±0.06	9.75±0.05	l,m,n
1RXS J051043.2–031627	12.11±0.04	12.01±0.03	11.38±0.03	NO	10.57±0.04	10.08±0.03	9.73±0.02	9.65±0.03	b,c,p
RX J0511.7–0348	13.13±0.07	12.77±0.06	12.02±0.04	NO	11.01±0.04	10.34±0.03	9.87±0.02	9.81±0.02	a,b,c
RX J0512.3–0255	14.10±0.06	13.56±0.04	12.61±0.03	12.05±0.04	11.49±0.04	10.43±0.02	9.69±0.02	9.14±0.02	c,i

<sup>S</sup> Saturated object.

<sup>ND</sup> Object not detected.

<sup>NO</sup> Object not observed.

<sup>a</sup>  $UBV$  from observations carried out at the Catania Astrophysical Observatory (Section 2.1).

<sup>b</sup>  $I_C$  from TASS Mark IV catalogue (Droege et al. 2006).

<sup>c</sup>  $JHKs$  from *2MASS* point source catalogue (Cutri et al. 2003).

<sup>d</sup>  $I_C$  from *DENIS* catalogue (Epchtein et al. 1997).

<sup>e</sup>  $U$  and  $B$  from Lee (1968);  $V$ ,  $R_C$ , and  $I_C$  from Taylor et al. (1989).

<sup>f</sup>  $U$  from Mundt & Bastian (1980).

<sup>g</sup>  $UBVR_CI_C$  from Vieira et al. (2003).

<sup>h</sup> Source blended with another star of similar brightness: the WFI  $BVR_CI_C$  photometry corresponds to the combined light of both stars.

<sup>i</sup> Weighted mean optical photometry from Cieslinski et al. (1997).

<sup>l</sup>  $BVR_CI_C$  from Alcalá et al. (1996).

<sup>m</sup>  $J$  from *DENIS* catalogue (Epchtein et al. 1997, converted to the 2MASS photometric system using the transformation equations provided by Carpenter (2001)).

<sup>n</sup>  $HKs$  from *2MASS* point source catalogue (Cutri et al. 2003).

<sup>p</sup>  $UBV$  from Frasca et al. (2003).

Table 4. Spectral type,  $H\alpha$  and Li I equivalent widths of the PMS stars in L1615/L1616. Additional emission lines observed in the spectra are also tabulated.

Star	SpT	W( $H\alpha$ ) ( $\text{\AA}$ )	W(Li) (m $\text{\AA}$ )	Type	Other emission lines	Notes
1RXS J045912.4–033711	G8	$1.80 \pm 0.20$	$355 \pm 10$	WTTS		a
1RXS J050416.9–021426	K3	$0.03 \pm 0.20$	$475 \pm 10$	WTTS		a
TTS 050513.5–034248	M5.5	$-9.80 \pm 0.40$	$800 \pm 100$	WTTS		
TTS 050538.9–032626	M3.5	$-4.90 \pm 0.20$	$350 \pm 20$	WTTS	He I	
RX J0506.6–0337	G9	$1.00 \pm 0.20$	$299 \pm 10$	WTTS		a
TTS 050644.4–032913	M4.5	$-4.70 \pm 0.30$	$560 \pm 40$	WTTS		
TTS 050646.1–031922	K4	$-41.00 \pm 2.00$	$560 \pm 20$	CTTS	He I, [N II], [S II]	
RX J0506.8–0318	K8.5	$-3.80 \pm 0.20$	$570 \pm 30$	WTTS	He I	
TTS 050647.5–031910	M5.5	$-10.20 \pm 0.80$	$560 \pm 50$	WTTS		
RX J0506.8–0327	M3.5	$-6.75 \pm 0.20$	$470 \pm 10$	WTTS		
RX J0506.8–0305	M4.5	$-4.80 \pm 0.30$	$590 \pm 50$	WTTS	He I	
TTS 050649.8–031933	M3.5	$-15.50 \pm 1.00$	$540 \pm 50$	WTTS	He I, [O I]	
TTS 050649.8–032104	M1:	$-195.00 \pm 5.00$	$190 \pm 20$	CTTS	He I, Na I, [O I]	b
TTS 050650.5–032014	M6.5	$-14.00 \pm 1.00$	$680 \pm 40$	WTTS		
TTS 050650.7–032008	M4.5	$-26.00 \pm 0.50$	$620 \pm 50$	CTTS	He I, [O I], [N II], [S II]	
RX J0506.9–0319NW	M2.5	$-3.50 \pm 0.30$	$590 \pm 50$	WTTS		
RX J0506.9–0319SE	K5	$-4.80 \pm 0.50$	$470 \pm 10$	CTTS	[O I], [N II], [S II]	
HD 293815	B9V	$8.60 \pm 0.50$				c
RX J0506.9–0320W	K8.5	$-2.90 \pm 0.50$	$500 \pm 20$	WTTS		
RX J0506.9–0320E	K0	$-1.50 \pm 0.50$	$380 \pm 10$	WTTS		
TTS 050654.5–032046	M4	$-60.00 \pm 5.00$		CTTS		
LkH $\alpha$ 333	K4	$-60.00 \pm 2.00$	$430 \pm 10$	CTTS	He I, [O I], [S II]	
L1616 MIR4	K1	$-60.00 \pm 6.00$	$370 \pm 50$	CTTS	[O I], [N II], [S II]	
Kiso A-0974 15	B3e	$-67.50 \pm 1.00$		HAeBe		e
RX J0507.0–0318	M0	$-2.00 \pm 0.50$	$570 \pm 30$	WTTS		
TTS 050657.0–031640	M4.5	$-94.00 \pm 2.00$	$430 \pm 40$	CTTS	He I, [O I]	
TTS 050704.7–030241	M6	$-17.50 \pm 1.00$	$740 \pm 50$	WTTS		
TTS 050705.3–030006	M0	$-2.00 \pm 0.40$	$400 \pm 20$	WTTS		
RX J0507.1–0321	M1	$-38.50 \pm 3.00$	$590 \pm 20$	CTTS	He I, [O I]	
TTS 050706.2–031703	M6	$-13.50 \pm 0.50$	$730 \pm 50$	WTTS		
RX J0507.2–0323	K4	$-1.10 \pm 0.10$	$480 \pm 20$	WTTS		
TTS 050713.5–031722	K8.5	$-10.50 \pm 0.50$	$520 \pm 30$	CTTS		
RX J0507.3–0326	M0	$-1.90 \pm 0.20$	$550 \pm 10$	WTTS		
TTS 050717.9–032433	M2.5	$-3.50 \pm 0.50$	$470 \pm 10$	WTTS		
RX J0507.4–0320	M4	$-5.00 \pm 0.50$	$530 \pm 50$	WTTS	He I	
RX J0507.4–0317	M3	$-14.50 \pm 0.50$	$510 \pm 50$	WTTS	He I	

Table 4—Continued

Star	SpT	W(H $\alpha$ ) ( $\text{\AA}$ )	W(Li) (m $\text{\AA}$ )	Type	Other emission lines	Notes
TTS 050729.8–031705	M6.5	$-12.00 \pm 0.50$	$450 \pm 20$	WTTS		
TTS 050730.9–031846	M5.5	$-290.00 \pm 30.00$		CTTS	He I	
TTS 050733.6–032517	M5.5	$-2.30 \pm 0.20$	$610 \pm 20$	WTTS		
TTS 050734.8–031521	M5	$-6.80 \pm 0.40$	$610 \pm 50$	WTTS	He I	
RX J0507.6–0318	K7	$-1.60 \pm 0.20$	$520 \pm 50$	WTTS		
TTS 050741.0–032253	M4	$-4.30 \pm 0.10$	$540 \pm 20$	WTTS		
TTS 050741.4–031507	M4.5	$-6.80 \pm 0.40$	$550 \pm 20$	WTTS		
TTS 050752.0–032003	M5.5	$-9.50 \pm 0.20$	$530 \pm 30$	WTTS		
TTS 050801.4–032255	M0.5	$-21.50 \pm 0.50$	$510 \pm 25$	CTTS	He I, [S II]	a
TTS 050801.9–031732	M1	$-15.50 \pm 0.50$	$410 \pm 25$	CTTS	He I, [S II]	a
TTS 050804.0–034052	M2.5	$-2.20 \pm 0.20$	$410 \pm 20$	WTTS		a
TTS 050836.6–030341	M1.5	$-68.50 \pm 1.00$	$560 \pm 30$	CTTS	He I	a
TTS 050845.1–031653	M3.5	$-6.70 \pm 1.00$	$530 \pm 50$	WTTS		
RX J0509.0–0315	G8	$1.10 \pm 0.20$	$320 \pm 10$	WTTS		a
RX J0510.1–0427	K4	$-0.20 \pm 0.20$	$230 \pm 10$	WTTS		a
1RXS J051011.5–025355	K0	$-0.10 \pm 0.20$	$415 \pm 10$	WTTS		a
RX J0510.3–0330	G8	$1.50 \pm 0.20$	$320 \pm 10$	WTTS		a
1RXS J051043.2–031627	G2	$2.40 \pm 0.20$	$235 \pm 10$	WTTS		a
RX J0511.7–0348	K1	$1.80 \pm 0.20$	$370 \pm 15$	WTTS		a
RX J0512.3–0255	K2	$-6.50 \pm 0.50$	$440 \pm 10$	CTTS		a

<sup>a</sup>W(H $\alpha$ ) and W(Li) from Alcalá et al. (2004).

<sup>b</sup>Veiled CTTS.

<sup>c</sup>Spectral type from Sharpless (1952).

<sup>e</sup>Spectral type from Vieira et al. (2003).

Table 5. Stellar parameters of the PMS stars in L1615/L1616.

PMS Star	$\log T_{eff}$	$R_V$	$A_V$ (mag)	$R_\star$ ( $R_\odot$ )	$\log L/L_\odot$
1RXS J045912.4–033711	$3.746 \pm 0.009$	$3.1 \pm 0.1^*$	$0.30 \pm 0.12$	$2.63 \pm 0.12$	$0.78 \pm 0.05$
1RXS J050416.9–021426	$3.675 \pm 0.014$	$3.1 \pm 0.1^*$	$0.35 \pm 0.22$	$2.35 \pm 0.11$	$0.40 \pm 0.07$
TTS 050513.5–034248	$3.494 \pm 0.010$	$3.1 \pm 0.1^*$	$0.49 \pm 0.20$	$0.55 \pm 0.03$	$-1.60 \pm 0.06$
TTS 050538.9–032626	$3.531 \pm 0.009$	$3.1 \pm 0.1^*$	$0.05 \pm 0.10$	$1.08 \pm 0.05$	$-0.85 \pm 0.05$
RX J0506.6–0337	$3.733 \pm 0.013$	$3.1 \pm 0.1^*$	$0.05 \pm 0.10$	$1.92 \pm 0.09$	$0.45 \pm 0.06$
TTS 050644.4–032913	$3.513 \pm 0.009$	$3.1 \pm 0.1^*$	$0.00 \pm 0.05$	$1.00 \pm 0.05$	$-0.99 \pm 0.05$
TTS 050646.1–031922	$3.662 \pm 0.026$	$4.2 \pm 0.4$	$4.33 \pm 0.35$	$1.91 \pm 0.11$	$0.17 \pm 0.11$
RX J0506.8–0318	$3.597 \pm 0.008$	$3.1 \pm 0.1^*$	$0.00 \pm 0.05$	$1.62 \pm 0.07$	$-0.24 \pm 0.05$
TTS 050647.5–031910	$3.494 \pm 0.010$	$3.0 \pm 0.2$	$2.30 \pm 0.17$	$1.03 \pm 0.05$	$-1.04 \pm 0.05$
RX J0506.8–0327	$3.531 \pm 0.009$	$3.1 \pm 0.1^*$	$0.44 \pm 0.10$	$2.43 \pm 0.11$	$-0.15 \pm 0.05$
RX J0506.8–0305	$3.513 \pm 0.009$	$3.1 \pm 0.1^*$	$0.05 \pm 0.10$	$1.28 \pm 0.06$	$-0.78 \pm 0.05$
TTS 050649.8–031933	$3.531 \pm 0.009$	$4.1 \pm 0.4$	$1.67 \pm 0.10$	$2.04 \pm 0.09$	$-0.30 \pm 0.05$
TTS 050649.8–032104	$3.573 \pm 0.008$	$3.1 \pm 0.1^*$	$4.72 \pm 0.12$	$2.29 \pm 0.10$	$-0.03 \pm 0.05$
TTS 050650.5–032014	$3.476 \pm 0.008$	$1.7 \pm 0.1$	$2.93 \pm 0.19$	$1.30 \pm 0.06$	$-0.91 \pm 0.05$
TTS 050650.7–032008	$3.513 \pm 0.009$	$3.4 \pm 0.2$	$2.20 \pm 0.17$	$1.28 \pm 0.06$	$-0.78 \pm 0.05$
RX J0506.9–0319NW	$3.549 \pm 0.008$	$3.1 \pm 0.1^*$	$0.00 \pm 0.05$	$1.22 \pm 0.05$	$-0.68 \pm 0.05$
RX J0506.9–0319SE	$3.622 \pm 0.025$	$4.1 \pm 0.4$	$1.62 \pm 0.49$	$2.78 \pm 0.14$	$0.33 \pm 0.11$
HD 293815	$4.021 \pm 0.049$	$3.5 \pm 0.5$	$0.76 \pm 0.05$	$2.03 \pm 0.09$	$1.65 \pm 0.20$
RX J0506.9–0320W	$3.597 \pm 0.008$	$2.4 \pm 0.2$	$2.24 \pm 0.12$	$3.98 \pm 0.18$	$0.54 \pm 0.05$
RX J0506.9–0320E	$3.720 \pm 0.014$	$3.3 \pm 0.1$	$4.72 \pm 0.15$	$3.65 \pm 0.17$	$0.96 \pm 0.07$
TTS 050654.5–032046	$3.522 \pm 0.009$	$3.1 \pm 0.1^*$	$4.33 \pm 0.10$	$0.58 \pm 0.03$	$-1.42 \pm 0.05$
LkH $\alpha$ 333	$3.662 \pm 0.026$	$3.1 \pm 0.1^*$	$2.60 \pm 0.44$	$3.92 \pm 0.29$	$0.79 \pm 0.12$
L1616 MIR4	$3.706 \pm 0.015$	$4.1 \pm 0.1$	$7.09 \pm 0.15$	$2.45 \pm 0.12$	$0.56 \pm 0.07$
Kiso A-0974 15	$4.272 \pm 0.058$	$5.5 \pm 0.1$	$5.20 \pm 0.20$	$2.59 \pm 0.15$	$2.87 \pm 0.24$
RX J0507.0–0318	$3.589 \pm 0.008$	$4.2 \pm 0.5$	$1.08 \pm 0.15$	$2.56 \pm 0.12$	$0.13 \pm 0.05$
TTS 050657.0–031640	$3.513 \pm 0.009$	$3.1 \pm 0.1^*$	$0.44 \pm 0.12$	$1.30 \pm 0.06$	$-0.76 \pm 0.05$
TTS 050704.7–030241	$3.484 \pm 0.009$	$2.5 \pm 0.4$	$0.74 \pm 0.47$	$0.71 \pm 0.08$	$-1.41 \pm 0.10$
TTS 050705.3–030006	$3.589 \pm 0.008$	$3.1 \pm 0.1^*$	$0.00 \pm 0.05$	$1.25 \pm 0.06$	$-0.49 \pm 0.05$
RX J0507.1–0321	$3.573 \pm 0.008$	$3.1 \pm 0.1^*$	$0.49 \pm 0.15$	$1.55 \pm 0.07$	$-0.37 \pm 0.05$
TTS 050706.2–031703	$3.484 \pm 0.009$	$3.0 \pm 0.1$	$0.88 \pm 0.22$	$0.78 \pm 0.04$	$-1.33 \pm 0.06$
RX J0507.2–0323	$3.662 \pm 0.026$	$3.1 \pm 0.1^*$	$0.25 \pm 0.22$	$1.53 \pm 0.07$	$-0.03 \pm 0.11$
TTS 050713.5–031722	$3.597 \pm 0.008$	$3.1 \pm 0.1^*$	$1.18 \pm 0.15$	$0.79 \pm 0.04$	$-0.86 \pm 0.05$
RX J0507.3–0326	$3.589 \pm 0.008$	$3.1 \pm 0.1^*$	$0.00 \pm 0.05$	$2.23 \pm 0.10$	$0.01 \pm 0.05$
TTS 050717.9–032433	$3.549 \pm 0.008$	$3.1 \pm 0.1^*$	$0.00 \pm 0.05$	$1.09 \pm 0.05$	$-0.77 \pm 0.05$
RX J0507.4–0320	$3.522 \pm 0.009$	$3.1 \pm 0.1^*$	$0.20 \pm 0.10$	$1.68 \pm 0.08$	$-0.51 \pm 0.05$
RX J0507.4–0317	$3.540 \pm 0.009$	$3.1 \pm 0.1^*$	$0.00 \pm 0.05$	$1.04 \pm 0.05$	$-0.85 \pm 0.05$

Table 5—Continued

PMS Star	$\log T_{eff}$	$R_V$	$A_V$ (mag)	$R_\star$ ( $R_\odot$ )	$\log L/L_\odot$
TTS 050729.8–031705	$3.476 \pm 0.008$	$2.5 \pm 0.1$	$1.32 \pm 0.19$	$0.73 \pm 0.03$	$-1.42 \pm 0.05$
TTS 050730.9–031846	$3.494 \pm 0.010$	$3.1 \pm 0.1^*$	$1.81 \pm 0.15$	$0.33 \pm 0.01$	$-2.02 \pm 0.05$
TTS 050733.6–032517	$3.494 \pm 0.010$	$3.1 \pm 0.1^*$	$0.54 \pm 0.20$	$0.69 \pm 0.03$	$-1.39 \pm 0.06$
TTS 050734.8–031521	$3.504 \pm 0.009$	$3.1 \pm 0.1^*$	$0.05 \pm 0.10$	$0.67 \pm 0.03$	$-1.37 \pm 0.05$
RX J0507.6–0318	$3.604 \pm 0.008$	$3.1 \pm 0.1^*$	$0.00 \pm 0.05$	$1.26 \pm 0.06$	$-0.43 \pm 0.05$
TTS 050741.0–032253	$3.522 \pm 0.009$	$3.1 \pm 0.1^*$	$0.05 \pm 0.10$	$1.02 \pm 0.05$	$-0.94 \pm 0.05$
TTS 050741.4–031507	$3.513 \pm 0.009$	$3.1 \pm 0.1^*$	$0.05 \pm 0.07$	$1.00 \pm 0.05$	$-0.99 \pm 0.05$
TTS 050752.0–032003	$3.494 \pm 0.010$	$3.1 \pm 0.1^*$	$0.64 \pm 0.20$	$0.74 \pm 0.03$	$-1.33 \pm 0.06$
TTS 050801.4–032255	$3.581 \pm 0.008$	$3.1 \pm 0.1^*$	$0.54 \pm 0.12$	$1.47 \pm 0.07$	$-0.39 \pm 0.05$
TTS 050801.9–031732	$3.573 \pm 0.008$	$3.1 \pm 0.1^*$	$0.39 \pm 0.12$	$1.46 \pm 0.07$	$-0.42 \pm 0.05$
TTS 050804.0–034052	$3.549 \pm 0.008$	$3.1 \pm 0.1^*$	$0.00 \pm 0.05$	$1.15 \pm 0.05$	$-0.73 \pm 0.05$
TTS 050836.6–030341	$3.565 \pm 0.008$	$3.1 \pm 0.1^*$	$0.64 \pm 0.10$	$1.97 \pm 0.09$	$-0.20 \pm 0.05$
TTS 050845.1–031653	$3.531 \pm 0.009$	$3.1 \pm 0.1^*$	$0.00 \pm 0.05$	$1.61 \pm 0.07$	$-0.51 \pm 0.05$
RX J0509.0–0315	$3.746 \pm 0.009$	$3.1 \pm 0.1^*$	$0.00 \pm 0.05$	$2.62 \pm 0.12$	$0.78 \pm 0.05$
RX J0510.1–0427	$3.662 \pm 0.026$	$3.1 \pm 0.1^*$	$0.00 \pm 0.05$	$3.74 \pm 0.17$	$0.75 \pm 0.11$
1RXS J051011.5–025355	$3.720 \pm 0.014$	$3.1 \pm 0.1^*$	$0.60 \pm 0.22$	$2.37 \pm 0.11$	$0.59 \pm 0.07$
RX J0510.3–0330	$3.746 \pm 0.009$	$3.1 \pm 0.1^*$	$0.10 \pm 0.08$	$2.16 \pm 0.10$	$0.61 \pm 0.05$
1RXS J051043.2–031627	$3.768 \pm 0.004$	$3.1 \pm 0.1^*$	$0.00 \pm 0.05$	$2.25 \pm 0.10$	$0.73 \pm 0.04$
RX J0511.7–0348	$3.706 \pm 0.015$	$3.1 \pm 0.1^*$	$0.00 \pm 0.10$	$2.40 \pm 0.11$	$0.54 \pm 0.07$
RX J0512.3–0255	$3.690 \pm 0.016$	$3.1 \pm 0.1^*$	$0.00 \pm 0.10$	$1.99 \pm 0.10$	$0.31 \pm 0.08$

\*Assumed (see Section 5.3).

Table 6: Effective wavelengths and absolute flux calibration constants for the Johnson-Cousins and 2MASS passbands. The main reference papers are listed in the last column.

Filter	$\lambda_{eff}$ ( $\mu\text{m}$ )	$F_{\lambda}^0$ ( $\text{erg/s}^2/\text{cm}^2/\text{\AA}$ )	Reference
$U_J$	0.36	$4.350 \cdot 10^{-9}$	Johnson (1965)
$B_J$	0.44	$7.200 \cdot 10^{-9}$	Johnson (1965)
$V_J$	0.55	$3.920 \cdot 10^{-9}$	Cousins (1976)
$R_C$	0.64	$2.254 \cdot 10^{-9}$	Cousins (1976)
$I_C$	0.79	$1.196 \cdot 10^{-9}$	Cousins (1976)
$J$	1.24	$3.129 \cdot 10^{-10}$	Cohen et al. (2003)
$H$	1.66	$1.133 \cdot 10^{-10}$	Cohen et al. (2003)
$K_s$	2.16	$4.283 \cdot 10^{-11}$	Cohen et al. (2003)



Table 7. Masses and ages for the PMS stars in L1615/L1616 as inferred by the evolutionary models by Baraffe et al. (1998) & Chabrier et al. (2000), D’Antona & Mazzitelli (1997) and Palla & Stahler (1999).

PMS Star	$M_{Ba98+Ch00}$ ( $M_{\odot}$ )	$Age_{Ba98+Ch00}$ (Myr)	$M_{DM97}$ ( $M_{\odot}$ )	$Age_{DM97}$ (Myr)	$M_{PS99}$ ( $M_{\odot}$ )	$Age_{PS99}$ (Myr)
1RXS J045912.4–033711	> 1.40	–	2.00	5.00	1.70	3.50
1RXS J050416.9–021426	> 1.40	–	0.95	0.70	1.60	3.00
TTS 050513.5–034248	0.12	6.00	0.17	10.00	0.14	10.00
TTS 050538.9–032626	0.35	4.04	0.25	2.20	0.26	2.80
RX J0506.6–0337	1.35	14.00	1.65	5.50	1.40	8.00
TTS 050644.4–032913	0.25	3.17	0.20	2.50	0.19	2.70
TTS 050646.1–031922	> 1.40	–	0.75	1.00	1.35	4.00
RX J0506.8–0318	1.05	5.00	0.50	1.00	0.68	3.00
TTS 050647.5–031910	0.18	2.00	0.16	2.00	0.13	2.00
RX J0506.8–0327	0.55	< 1.00	0.20	0.10	0.25	0.40
RX J0506.8–0305	0.26	1.78	0.19	1.50	0.18	1.50
TTS 050649.8–031933	0.47	1.00	0.22	0.20	0.25	0.70
TTS 050649.8–032104	0.87	1.30	0.35	0.40	0.50	0.80
TTS 050650.5–032014	0.09	< 1.00	0.13	1.00	< 0.10	0.70
TTS 050650.7–032008	0.26	1.60	0.19	1.50	0.18	1.50
RX J0506.9–0319NW	0.50	4.50	0.33	2.00	0.35	2.50
RX J0506.9–0319SE	1.40	1.30	0.45	0.30	0.93	0.80
HD 293815	> 1.40	–	2.50	3.00	2.50	3.00
RX J0506.9–0320W	1.25	< 1.00	0.32	0.07	0.68	0.40
RX J0506.9–0320E	> 1.40	–	2.30	0.90	2.30	1.50
TTS 050654.5–032046	0.26	14.20	0.25	14.00	0.22	10.00
LkH $\alpha$ 333	> 1.40	–	0.75	0.20	1.70	0.50
L1616 MIR4	> 1.40	–	1.70	1.70	1.75	3.00
Kiso A-0974 15	> 1.40	–	> 3.00	–	5.50	0.30
RX J0507.0–0318	1.10	1.45	0.35	0.30	0.60	0.80
TTS 050657.0–031640	0.27	1.60	0.19	1.50	0.18	1.50
TTS 050704.7–030241	0.11	3.00	0.15	4.50	0.10	3.00
TTS 050705.3–030006	0.90	10.05	0.55	3.00	0.63	4.50
RX J0507.1–0321	0.80	4.30	0.40	1.00	0.50	2.50
TTS 050706.2–031703	0.12	2.55	0.15	4.00	0.10	2.50
RX J0507.2–0323	1.25	11.30	0.85	2.00	1.20	7.50
TTS 050713.5–031722	0.73	35.80	0.70	20.00	0.60	20.00
RX J0507.3–0326	1.05	2.00	0.37	0.40	0.60	0.80
TTS 050717.9–032433	0.50	6.32	0.34	2.80	0.35	3.00
RX J0507.4–0320	0.36	1.13	0.20	0.70	0.22	0.80
RX J0507.4–0317	0.42	5.50	0.28	2.80	0.31	3.00

Table 7—Continued

PMS Star	$M_{Ba98+Ch00}$ ( $M_{\odot}$ )	$Age_{Ba98+Ch00}$ (Myr)	$M_{DM97}$ ( $M_{\odot}$ )	$Age_{DM97}$ (Myr)	$M_{PS99}$ ( $M_{\odot}$ )	$Age_{PS99}$ (Myr)
TTS 050729.8–031705	0.09	2.53	0.13	4.00	< 0.10	3.00
TTS 050730.9–031846	0.11	20.11	0.15	30.00	0.13	30.00
TTS 050733.6–032517	0.14	4.00	0.17	5.50	0.13	4.00
TTS 050734.8–031521	0.17	5.65	0.20	6.50	0.16	5.00
RX J0507.6–0318	1.00	11.27	0.62	3.00	0.75	7.00
TTS 050741.0–032253	0.30	3.60	0.23	2.50	0.22	2.50
TTS 050741.4–031507	0.25	3.17	0.20	2.50	0.18	2.50
TTS 050752.0–032003	0.15	3.56	0.17	4.50	0.13	3.00
TTS 050801.4–032255	0.88	5.67	0.47	1.60	0.56	3.00
TTS 050801.9–031732	0.80	5.02	0.44	1.50	0.50	2.70
TTS 050804.0–034052	0.50	5.67	0.33	2.50	0.35	2.80
TTS 050836.6–030341	0.75	2.01	0.32	0.60	0.44	1.00
TTS 050845.1–031653	0.40	1.61	0.23	0.90	0.26	1.00
RX J0509.0–0315	> 1.40	–	2.00	4.50	1.75	3.50
RX J0510.1–0427	> 1.40	–	0.70	0.20	1.70	0.50
1RXS J051011.5–025355	> 1.40	–	1.85	2.50	1.65	4.00
RX J0510.3–0330	> 1.40	–	1.70	7.00	1.50	6.00
1RXS J051043.2–031627	> 1.40	–	1.65	8.00	1.50	6.50
RX J0511.7–0348	> 1.40	–	1.70	2.00	1.70	4.00
RX J0512.3–0255	> 1.40	–	1.30	2.00	1.50	5.00

Table 8.  $\alpha$  slopes of the IMF in different clusters and associations.

Cluster	Age (Myr)	Mass range ( $M_{\odot}$ )	$\alpha$	Ref.
M35	150	0.1-0.4	0.58	a
$\alpha$ Per	80	0.06-0.2	0.56	b
Pleiades	120	0.03-0.45	$0.60 \pm 0.11$	c
$\lambda$ Orionis	5	0.02-1.2	$0.60 \pm 0.06$	d
$\sigma$ Orionis	5	0.013-0.2	$0.8 \pm 0.4$	e
Trapezium	0.4	0.035-0.56 0.25-3	$\sim 0.3$ $\sim 0.7$	f
$\rho$ Oph	0.1-1	0.02-0.4	$\sim 0.5$	g
IC 348	3	0.035-0.5	$0.7 \pm 0.2$	h
Taurus-Auriga	1-2	0.08-1	1.35	i
Cha I	$\approx 3$	0.08-1.2	0.6-1.1	j, k
Cha II	2-5	0.1-1	0.5-0.6	l
L1615/L1616	1-3	0.1-5.5	$0.84 \pm 0.07$	This work

References. — a) Barrado Y Navascuès et al. (1998); b) Barrado Y Navascuès et al. (2002); c) Moraux et al. (2003); d) Barrado Y Navascuès et al. (2004b); e) Bèjar et al. (2001); f) Luhman et al. (2000); g) Luhman & Rieke (1999); h) Tej et al. (2002); i) Briceño et al. (2002); j) López Martí et al. (2004); k) Comerón et al. (2000); l) Spezzi et al. (2008).